Civil and Natural Resources Engineering

UC UNIVERSITY OF CANTERBURY
Te Whare Wānanga o Waitaha
CHRISTCHURCH NEW ZEALAND

Biennial Project 08/548

Debris flow mechanics for New Zealand mountain catchments

Report prepared for the New Zealand Earthquake Commission (EQC)

Project Leader: Dr. Elisabeth Bowman

Co-Investigator: Patrick Kailey

Department of Civil and Natural Resources Engineering
University of Canterbury, August 2010

TABLE OF CONTENTS

EXECUTIVE SUMMARY

PLAIN ENGLISH SUMMARY

CHAPTER 1: INTRODUCTION

1.1 Project objectives 3

1.2 Report organisation 4

1.2 Future outputs and capacity building 4

CHAPTER 2: FIELD INVESTIGATIONS OF TWENTY DEBRIS FLOWS

2.1 Introduction 3

2.2 Methods 4

2.3 Field investigation summary 8

2.3.1 Southern Rimutaka (Orongorongo) Field Area 9

2.3.2 Cass Field Area 14

2.3.3 Birch Hill Field Area 17

2.3.4 Franz Joseph Field Area 21

2.4 Discussion and Conclusions 23

Acknowledgements 26

REFERENCES 27

CHAPTER 2: PHYSICAL MODELLING OF DEBRIS FLOWS ON THE CENTRIFUGE 29

3.1 Introduction 30

3.1.1 Physical modelling of debris flows 30

3.1.2 Volume, moisture content and velocity effects 30

3.1.3 Pore fluid effects 31

3.2 Geotechnical centrifuge tests 31

3.2.1 Concept 31

3.2.2 Programme 32

3.3 Centrifuge testing 33

3.3.1 Apparatus and instrumentation 33

3.3.2 Centrifuge scaling principles 35

3.3.3 Pore fluid 36

3.3.4 Material constraints 37

3.4 Test results 39

3.4.1 High speed camera imagery and flow heights 39

3.4.2 Flow velocity 40

3.4.3 Velocity profiles 43

3.4.4 Flow discharge 45

3.4.5 Runout and deposition 50

3.5 Discussion and conclusions 56

Acknowledgements 57

REFERENCES 58

EXECUTIVE SUMMARY

Debris flows, high speed, gravity-driven mixtures of soil, rock and water, are ubiquitous mass-wasting processes in areas of high relief and rainfall. New Zealand's position in the mid-latitudes of the Pacific Ocean results in periods of high-intensity rainfall – leading to high rates of physical weathering. Combined with extremely high rates of uplift and highly indurated, fractured bedrock, these factors result in a particularly high temporal occurrence of debris flows. Despite the danger they pose, the public recognition of the losses wrought by debris flows is relatively low in New Zealand. This is largely a result of the country's low population density, especially in regions most prone to them. This situation is gradually changing as hilly and mountainous terrain, once thought marginal, is developed.

Despite some notable examples of large debris flows, such as that which occurred at Matata in the Bay of Plenty in May 2005, the state of knowledge on New Zealand specific debris flow occurrence is sparse. While there has been some qualitative work done on specific cases, there has been very little detailed quantitative assessment of these hazards in New Zealand. To address this, a detailed field investigation of twenty debris flows covering four regions within New Zealand was undertaken. The flows examined were located in the North Island in the Southern Rimutaka Mountains and in the South Island, near Cass, Mt Cook and Franz Joseph Glacier. These flows cover a wide range of debris flow types, from the bouldery, channelized events to little-studied, smaller, hill-slope debris flows. They also cover a wide range of geoclimatic conditions, from extremely high-rates of rainfall west of the Southern Alps to the comparatively drier conditions east of the divide. The methodology used to map the debris flows was adapted from that used extensively in British Columbia, Canada. The method examines the flows on a reach-by-reach basis, with details of erosion and deposition being mapped as well as slope angles, channel widths, and flow thickness being measured or estimated from field evidence. Observations of constrictions in the flow path, the entry or exit of stream flow and other details help to provide a detailed picture of the history and path of each flow.

Values of total deposition in the data-set range from 10,000 m^3 to 300 m^3, which is typically smaller than most of the event magnitudes discussed in the debris flow literature. The detailed investigation of small, non-anthropogenic induced events makes this New Zealand data-set unique. The results of the data can be further utilised in developing empirical models of runout for New Zealand specific conditions and can be compared with statistical-empirical models developed in similar conditions elsewhere. Details of each individual flow within a dataset can be examined to assess the influence of moisture and flow geometry on the overall behaviour. The aim is to determine the specific mechanisms that lead to departures of behaviour from the average within a locality and therefore to better understand the risks and uncertainties within each dataset.

While forensic field studies are invaluable in describing the flow behaviour typical of an area, they are less useful in elucidating the underlying mechanics of the behaviour,

as many important variables such as moisture content, the geotechnical properties of the material, and exact volumes are extremely difficult to determine after an event. Therefore, a series of physical modelling experiments using a small-scale flume housed within a geotechnical centrifuge was undertaken in parallel with the field component of the study. The focus of this study was to better understand the mechanisms underlying debris flow behaviour in general, by measuring and varying parameters of interest and carefully observing the result. .

The experiments were designed to examine the effect of varying the moisture content and flow volume on debris flow velocity, discharge, and runout. The effect of pore-fluid rheology was also examined by using both Newtonian and non-Newtonian pore fluids. Detailed measurements of pore pressure were taken at positions along the flume, while a high speed camera was used to capture the flow behaviour close to the exit of the confined flow to the unconfined fan area. Measurements were also taken of the thickness and extent of the deposition area and the flume bed after each test.

A strong linear correlation was found between peak flow momentum (defined as the product of the front velocity and total mass of the flow) and runout to the centre of gravity of the deposit. This was found to be better than the relationships between either the square of velocity or mass to runout, as found elsewhere in the literature. The results should be treated with caution at this stage, since the boundary conditions within the study may influence this result. The results also showed the pore fluid rheology to have a dramatic effect on the acceleration and deceleration of the flow within the channel. However, perhaps surprisingly, this is did not translate to a large difference in deposit morphology. In light of this, a discussion is made on the contrasting influences of pore fluid viscosity on consolidation and drag mechanics during downslope motion and flow arrest. It is possible that the dominance of different mechanisms of shear resistance shifts between channelized down-slope movement and unconfined runout, which will have important implications for both the understanding and modelling of debris flow behaviour.

PLAIN ENGLISH SUMMARY

Debris flows consist of mixtures of soil, rock and water that travel at high speeds down slopes – often within stream channels, but sometimes also on open slopes. They tend to occur frequently in mountainous areas when there is heavy rainfall and a good quantity of debris available, either from natural erosion supplied by weathering and small landslips, or from human activity such as logging. Debris flows may add to their volume by eroding material in their paths or may lose volume by depositing material as they travel downslope. Usually, they end on relatively shallow open slopes as a fan of debris. Unfortunately, often this is where infrastructure is built, including roads, houses and bridges.

Debris flows are common in New Zealand because of the high level of precipitation and the relatively weak rocks that make up the mountain landscape. Despite this, the public recognition of debris flows is relatively low in New Zealand because of its low population density, although this is gradually changing.

In New Zealand, there has been very little detailed assessment of debris flows in terms of how large they are, how far they run, what sort of materials are involved, how frequently they occur and how they are triggered. This knowledge is needed in order for risk assessment of these hazards to be carried out. To begin to address this, a study was conducted that included the detailed mapping of 20 debris flow events in relatively undisturbed areas (i.e. areas that had not been affected recently by wildfire or logging, for instance). The resulting data-set covers four regions of New Zealand, representing a wide-range of climatic conditions and geology. The information gleaned from this study is aimed at putting New Zealand's debris flows in the context of the world-wide state of knowledge, so that simple empirical and statistical models can be used for risk assessment and mitigation of these dangerous events.

While these field investigations are useful to place New Zealand flows in context and suggest reasonable methods of hazard assessment, they are not very useful in understanding the underlying physics of debris flow movement, as many important variables influencing the debris flow are unknown. To overcome this, a parallel study was conducted using a small-scale experimental debris flow channel housed within a geotechnical centrifuge. The small-scale of the experiment enabled debris flow behaviour to be examined in a carefully controlled manner, a situation that is not possible to achieve in the field, while the centrifuge allowed important processes to be scaled up to more closely model a larger debris flow in the field. In particular, these tests explored the influence of moisture and soil mass on debris flow velocity and travel distance. Sensors placed in the channel enabled the model flow to be tracked before it exited on the debris flow fan, while a camera was used to provide high speed footage of the flow. The results showed clear relationships between flow velocity, mass, momentum, slope, moisture and travel distance which can be used to give insight to debris flow mechanics and generate better models for risk mitigation.

CHAPTER 1: INTRODUCTION

1.1 PROJECT CONTEXT AND OBJECTIVES

This report is a summary of the outputs from a two-year study “Debris Flows for New Zealand Mountain Catchments”, which was funded as Biennial Research Project BIE 08/548 by the New Zealand Earthquake Commission, EQC. Dr Elisabeth Bowman was the project leader and Patrick Kailey, a postgraduate PhD research student at the University of Canterbury, acted as co-investigator. Additional assistance was provided by members of the University of Canterbury, GNS Science and the Swiss Federal University of Science and Technology, Zurich (ETH, Zurich) as detailed in the Acknowledgements section of each chapter.

Debris flows are one of the most dangerous mountain hazards in New Zealand. Recent debris flow disasters in Matata (Bay of Plenty), the Rees Valley (Otago), and the Wellington region evince their destructive potential. The May 18th 2005 debris flow event in Matata, in the Bay of Plenty, resulted in the destruction of 27 houses and damage to 87 further dwellings. While this debris flow was comparatively large, many smaller debris flows leading to lesser economic losses occur each year. As well as generating economic losses, a number of debris flows have claimed lives both historically and in recent years, including the Waihi events in 1846 and 1910, near Lake Taupo, which resulted in a combined loss of 66 lives; the Klondyke corner, Arthurs Pass debris flow of 1979 which claimed 4 lives; the Thames, Te Aroha event of 1985 which killed 3 people and the Rees Valley, West Otago, tragedy of 2002 in which one died.

It has been found to be instructive in other parts of the world to collate and compare materials, geometries and initiation events of individual debris flow events within a locality to understand the mechanics of most relevance and to develop of tools and techniques for risk evaluation. Physical modelling of debris can be used to develop a mechanical understanding of the influence of particular parameters on debris flow behaviour.

The overall aim of this project was to begin to link the hazard prediction of debris flows in New Zealand with a mechanical understanding of their behaviour. This aim was met via the following project objectives:

(1) To document characteristic debris flow events in New Zealand, based on a regional zonation with consideration of their distinctive materials and geomorphological and climatic setting.

(2) To increase mechanical understanding of debris flow behaviour in materials applicable to New Zealand using physical modelling, and in particular address the

role of channel geometry, soil type, flow quantity and moisture condition in determining the magnitude of debris flows downstream

(3) To determine scaling laws and empirical relationships for debris flows that would enable further modelling research to be carried out in New Zealand

1.2 REPORT ORGANISATION

The report consists of two main sections or chapters which focus on the two major elements of the work – a field survey of New Zealand debris flows and physical modelling of small scale debris flows.

Chapter 2 discusses the field survey of twenty debris flows within four regions of New Zealand, including methods and techniques used, the regions covered, and descriptions of characteristic flows for each region. An example of the data reach-by-reach data collected for one flow is given and the overall results in context of a global dataset of travel angle (ratio of vertical to horizontal distance travelled) versus debris flow size.

Chapter 3 discusses the physical modelling of nine model debris flows using a geotechnical drum centrifuge at ETH, Zurich. The chapter details the experimental arrangement, data collected and the analysis of data. Experimental variables in the tests described included total volume of flow, moisture content and fluid rheology. Focus is given to how these variables affect the overall runout or travel distance of the flows.

1.3 FUTURE OUTPUTS AND CAPACITY BUILDING

Patrick Kailey will continue to work on the data derived from the above as part of his PhD, which is otherwise funded through a University of Canterbury Doctoral Scholarship. The aim is a more in depth analysis of the data and comparison with statistical-empirical / mechanistic models from others.

Warren McKenzie and Angus Newsam are 3rd professional civil engineering students at the University of Canterbury, who provided assistance in undertaking fieldwork as part of Summer and final year projects, respectively.

Conference papers have been accepted for the 11th IAEG Congress to be held in Auckland in September 2010 and provisionally accepted for the 5th International Conference on Debris Flow Hazards Mitigation to be held in July 2011 in Padova, Italy. Papers are also being prepared for submission to journals.

CHAPTER 2: FIELD INVESTIGATIONS OF TWENTY DEBRIS FLOWS

ABSTRACT

This chapter summarizes the field investigation of twenty debris flow paths covering four regions within New Zealand; four in the Southern Rimutakas of the North Island, twelve in the vicinity of Cass, just east of Arthur's Pass National Park, three off the Ben Ohau Range in Mt. Cook National Park, and two flows near the Franz Joseph Glacier. The resulting data set covers a wide range of debris flow types and climatic conditions. Debris flows in the Southern Rimutakas are of the bouldery, channelized type and are most likely triggered by rockfall events in steep, bedrock source reaches. Debris flows in Cass are of the slope type, are typically smaller, and deposit on high slope angles. Debris flow behaviour at Mt. Cook is transitional between open, hill-slope type and channelized type and characterized by harder, more metamorphosed rock types than at Cass. Flows near Franz Joseph are of the channelized type, but appear to be characterized by a coarser particle size distribution and more woody vegetation in the depositional material than in other field areas. Values of total deposition in the data-set range from 10,000 to 300 m^3, which is typically smaller than most of the event magnitudes discussed in the debris flow literature. The detailed investigation of small, non-anthropogenic induced events makes this New Zealand data-set unique.

2.1 Introduction

Debris flows are one of the most dangerous mountain hazards in New Zealand. The micro-continent's rapid rates of uplift combined with its mid-latitude position in the path of the "Roaring Forties" creates many areas of steep topography with frequent, high-intensity rainfall—a situation ripe for producing debris flows. Recent debris flow disasters in Matata (Bay of Plenty), the Rees Valley (Otago), and the Wellington region evince the destructive potential of debris flows (McSaveney et al. 2006, McSaveney & Glassey 2006), however, New Zealand's low population density and sparse infrastructure in the most susceptible areas currently limit damage (McSaveney & Davies 2005).

Unfortunately, the danger posed by New Zealand's debris flows is likely to increase. As the country's population, tourism industry, and infrastructure continue to push further into mountainous terrain, understanding New Zealand's debris flows will become increasingly important. This study seeks to extend our understanding of New Zealand debris flow events by following two parallel and complementary methods of inquiry: field investigation and physical modelling.

Field investigation is the first step in this process. Surveying historical flows gives the hazard manager or engineer a tool for back analyses, a basis for engineering judgment, and the raw data for developing quantitative models. Despite the importance of field research, little work has been done to systematically characterize debris flows in New Zealand. This work begins to fill this gap in knowledge.

INITIAL RESEARCH QUESTIONS

- What types of debris flows are typical of New Zealand alpine catchments? What are the dominant factors controlling debris flow behaviour in each field area?
- How do New Zealand's debris flows compare to other debris flows around the world?
- What empirical models, generated for other localities, are appropriate to use in New Zealand, and in what circumstances?

2.2 Methods

The field studies began with an examination of NZ's topography and of the literature on NZ debris flows and discussions with other researchers, notably at GNS Science – Chris Massey and Mauri McSaveney and with Jonathan Fannin from University of British Columbia, Canada, who visited New Zealand on two occasions, one of which was specifically to take part in a debris flow field survey. Several field reconnaissance surveys were carried out in the early stages to examine potential debris flows sites for approximate age, accessibility and mappability, It was important to be able to characterise deposits that had not had extensive reworking – hence a limit on age of approximately 5 years. Some of the largest debris flows were difficult to access, particularly in their upper sections, while a number of flow deposits were cut and eroded by rivers, making these not practical for full mapping. The selected debris flow sites were those that fulfilled all three aforementioned criteria.

Once selected, in order to characterize each debris flow, each flow path was divided into a series of reaches based on similar geometry, materials, and flow behaviour (Fannin and Rollerson 1993). Length, width and channel geometry of each reach was measured using a laser rangefinder and chainage tape. Slope and azimuth of each reach were determined with an inclinometer and compass. GPS points taken at key points along the debris flow path enabled the chainage-length map to be geo-referenced onto appropriately scaled base-maps. An example of the data collected for Cass 11 is shown in Table 1.

Measuring channel geometry/morphology was straightforward, however, estimating depth of deposition and erosion from forensic evidence was more challenging because channel morphology prior to the flow had to be inferred. In places, buried paleosols or vegetation indicated the location of the original surface. Levees, strandlines/mudlines and debris in trees were used to estimate the flow height. A trim line – corresponding to erosion of the bed – was often observed on the channel bank, below which vegetation was removed and the bank recently disturbed. This line is key to estimating the depth of erosion by the passing flow. However, while the trim line may represent the original ground surface; it is unlikely that the original surface was completely flat. Rather, because the debris flows investigated here all developed pre-existing gullies, the channel probably had a U or V-shaped cross section before the event. Hence, the trim line may simply represent marginal widening of the channel as the flow travelled past. For this reason, whenever we were not confident of the original channel morphology, we estimated an upper and lower bound of erosion in each reach. The upper bound usually assumes a flat, box shaped channel with vertical erosion. The lower bound represents a scenario where the flow moved over an incised, v-shaped channel, marginally widening the channel into the u-shape that is more typical of a debris flow channel.

The distinction between separate debris flow events may also be difficult to determine. One debris flow surge may erode, while another may deposit in the same reach. Further, a small flow may strip evidence of relative age from clasts in the channel bed, causing an overestimate of deposition by the event in question. Despite these difficulties, we believe the error in volume balances presented is reasonable and within the ranges reported in other debris flow studies (Gartner et al 2008; Santi et al 2008, Conway et al 2009). Reporting an upper and lower bound also helps preserve and communicate the uncertainty in volume balance measurements.

*Table 1: Example of data collected for Cass11. *Flow behaviour was categorized as either erosion (E),transport (T), or depositional (D) **Confinement types were categorized as; confined in gully (CG), partially confined in channel (PCC), confined in channel (CC),unconfined (UC). Bed types are classified as veneer of colluvium over bedrock (veneer), slope colluvium (col), fan colluvium (fan col). UL abbreviates unlimited.*

General							Widths (m)				
Reach	Chainage Length (m)	Azimuth	Slope	Bend angle	Flow Behaviour*	Confinement type**	Gully	Channel	Trace	Deposition	Erosion
1	43	320	-34.4	0	E	CG/PCC	16	na	16	na	16
2	233	320	-34.4	0	E	CG	15	4	15	na	15
3	317	318	-33.4	2	T	CC	1	2	2	2	2
4	375	321	-33.5	-3	E	PCC/CG	8.9	4.1	4.1	4.1	2
5	430	320	-32.7	1	T/E	CC	5.1	3.5	3.5	4	3.5
6	496	318	-33.2	2	T/E	PCC	na	2.6	7.6	7.6	2.6
7	523	310	-31.9	8	T/E	CC	5	2.8	2.8	2.8	2.8
8	544	302	-32.6	8	T/E	CC	5	2.8	2.8	2.8	5
9	565	321	-28.8	-19	T/E	CC	5	2.8	2.8	2.8	2.8
10	590.2	321	-29.4	0	T/E	PCC	na	4.3	6.5	6.5	4.3
11	642.8	314	-29	7	T/E	PCC	na	3.4	7.2	7.2	3.4
12	668.8	314	-28.2	0	T/E	PCC	na	2.5	6.5	6.5	2.5
13	684.8	300	-30.5	14	T/E	PCC	na	2.5	7.2	7.2	2.5
14	712.8	324	-29.7	-24	T/E	PCC	na	2.4	4.8	4.8	2.4
15	733.1	318	-27.6	6	T/E	PCC	na	1.5	2.5	2.5	1.5
16	749.1	348	-26.6	-30	E	CC	na	3	7.1	7.1	3
17	766.6	21	-25	-33	T	CC	na	2.3	3.3	3.3	2.3
18	793	6	-22.6	15	E	CC	na	2.1	3.1	3.1	2.1
19	802	321	-18.3	45	D	CC	na	2.4	6.4	6.4	2.4
20	838.2	349	-17.2	17	D	UC	na	na	16	16	na

continued	Heights (m)				Erosion (m^3)				
Type of deposition	Channel	Channelized by?	Flow	Gully	Upper bound	Lower bound	Deposition (m^3)	Bed type***	Debris availability
na	na	na	0.1	0.1	69	69	0	veneer	0-.5m
na	2	Gulley	2.5	2.5	980	143	0	col	0-2m
thin, inset levees	2.5	channel	1	2.5	84	28	42	col	0-2m
thin, inset levees	2	Gulley, then levees	1.5	2.4	174	58	56	col	UL*
thin, inset levees	1.7	Gulley/channel	1.3	1.7	144	48	19	col	UL
thin, inset levees	1.6	Channel	1.6	na	50	16	24	col	UL
thin discontinous levees	1.7	Channel	1	na	34	11	5	col	UL
thin discontinous levees	2	Channel	1	na	29	10	4	col	UL
thin discontinous levees	2	Channel	1	na	29	10	4	col	UL
levees	1	Channel	1	na	38	13	17	col	UL
levees	1.2	Channel	1.2	na	79	26	35	col	UL
levees	1.3	Channel	1.4	na	42	0	34	col	UL
levees	1.3	Channel	1.8	na	26	0	20	col	UL
levees	1.3	Channel	1.5	na	44	0	13	col	UL
levees	1.3	Channel	1.4	na	20	0	2	col	UL
levees	1.5	Channel	1.5	na	24	0	1	col	UL
levees	1	Channel	1	na	9	0	5	col	UL
levees	1	Channel	1	na	28	0	4	col	UL
levees	1.4	own levees	1.4	na	3	0	16	fan col.	UL
remoulded lobe	na	unconfined	1.5	na	0	0	144	fan col.	UL

2.3 Field investigation summary

The following chapter summarizes field investigation of twenty debris flow paths; four in the Southern Rimutakas of the North Island, twelve in the vicinity of Cass, just east of Arthur's Pass National Park, three off the Ben Ohau Range in Mt. Cook National Park, and two flows near the Franz Joseph Glacier (Figure 1). Volumes of deposition and travel angles are shown in Table 2. The resulting data set covers a wide range of debris flow types and climatic conditions.

*Table 2 Summary of flows surveyed from 2008-2010 field seasons. Length (L) is measured along the horizontal from inferred starting location to end of deposition. * Travel angle is defined as tan (L of travel of coarse clastic material/fall height of coarse clastic). Parentheses indicate the travel angle calculated for all deposition material, including outwash and remoulded material.*

Flow code	Total deposition (m^3)	Deposition past last confined reach (m^3)	Travel angle* (°)	Length of travel (m)
OR1	10810	7610	31	920
OR2	2095	1524	23	930
OR3	5490	4930	25	550
OR4	3990	3550	50	380
Cass1	756	76	25	870
Cass2	726	231	36	410
Cass3	3000	2426	30	1120
Cass6	2350	2300	43 (43)	689
Cass7	880	840	37 (33)	920
Cass10	2850	2600	17 (17)	425
Cass11	450	160	41 (39)	715
Cass12	2920	2740	29 (29)	820
Cass13	1330	580	26 (20)	880
Cass14	570	540	25 (20)	790
Cass15	2700	1864	30 (17)	1120
BH1	336	14	38 (38)	707
BH2	640	420	32 (31)	480
BH3	1350	750	28 (23)	960
FJ3	2480	2000	27 (27)	580
FJ4	1380	636	28 (28)	490

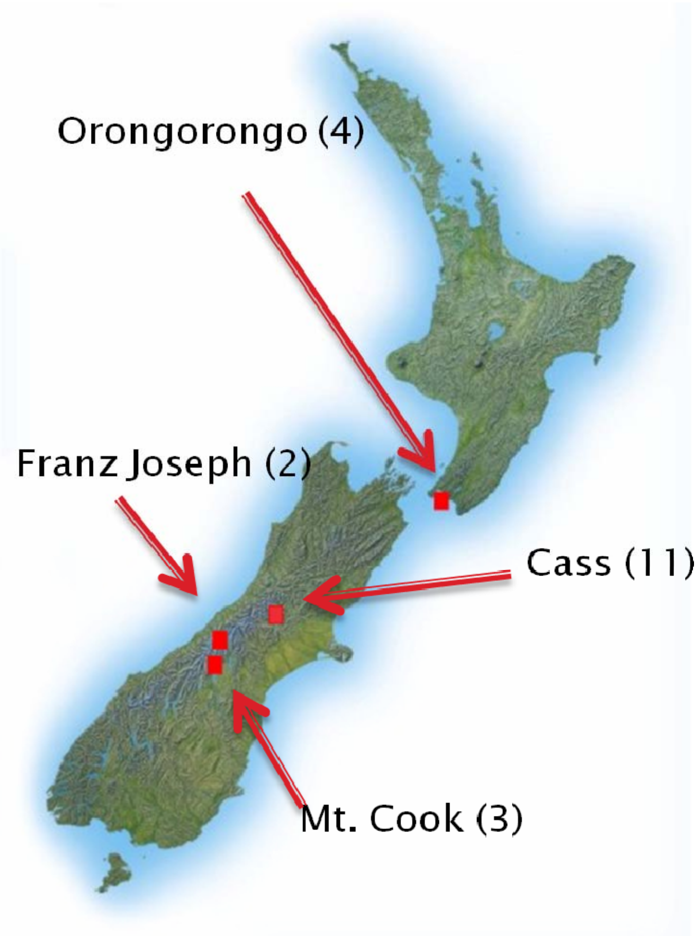

Figure 1 Location of field sites within New Zealand and numbers of flows mapped.

2.3.1 Southern Rimutaka (Orongorongo) Field Area

Debris flows in the southern Rimutakas (termed the Orongorongo study area) source from outcrops of deeply indurated, deformed Mesozoic greywacke with limited interbeds of conglomerate, argillite, and mudstone. The Rimutakas themselves are part of an anticline associated with thrusting of the Wairarapa reverse fault to the west, which runs parallel to the range. Fault ruptures have created a spectacular set of beach terraces in the area, the last of which was formed during the 1855 Wairarapa Earthquake (Begg & McSaveney 2005). The rapid uplift rates supplied by the fault, direct exposure to frequent southerly storms, and the unstable nature of the bedrock make debris flows in these catchments frequent events. Based on the amount of vegetation on observed debris flow fans, it appears that flows reaching the distal ends of the fans occur within at least decadal intervals. Smaller flows that recharge lower reaches near the fan heads occur even more regularly, perhaps each year or two.

In October and November 2008, four debris flows were investigated. Shorter flows such as OR4 only took one field day to map, whereas OR1 and OR2 required over four field days each.

The Orongorongo flows belong to the channelized, bouldery type debris flows that dominate the debris flow literature (Hungr et al. 2001, Jakob 2005, Rickenmann 1999). From their initial source high on the bedrock headwalls, the Orongorongo events entrain moderate amounts of coarse colluvium before entering the main channel. Once joining the main stem, most flows entrain enough fines from valley colluvium and water from nearly perennial stream flow to mobilize into mature debris flows. Note that debris flow OR4 may be an exception, as limited stream flow may have contributed to a lower moisture content, which may explain the exceptionally high travel angle shown in Table 2. The lack of any remoulded or fluvial reworked material beyond the main zone of clastic deposition supports this interpretation.

Figure 2 presents a geomorphic model of debris flow OR1. In this figure, Zone (a) is a reworked deposition and fluvial outwash area, representing material that was reworked by hyperconcentrated flow and fluvial processes during or post event; Zone (b) indicates the deposition of coarse colluvium, which is the final extent of most the material deposited by the debris flow; Zone (c) is a distinct zone of erosion occurring at the fan-head; Zone (d) is a transport zone, where lateral scree slopes and bank failure quickly recharge channel, while variable erosion and deposition occur in response to channelization and particle jamming; finally Zone (e) is the source area(s) where rockfall entrains limited amounts of colluvium from bedrock depressions before joining the main-stem channel.

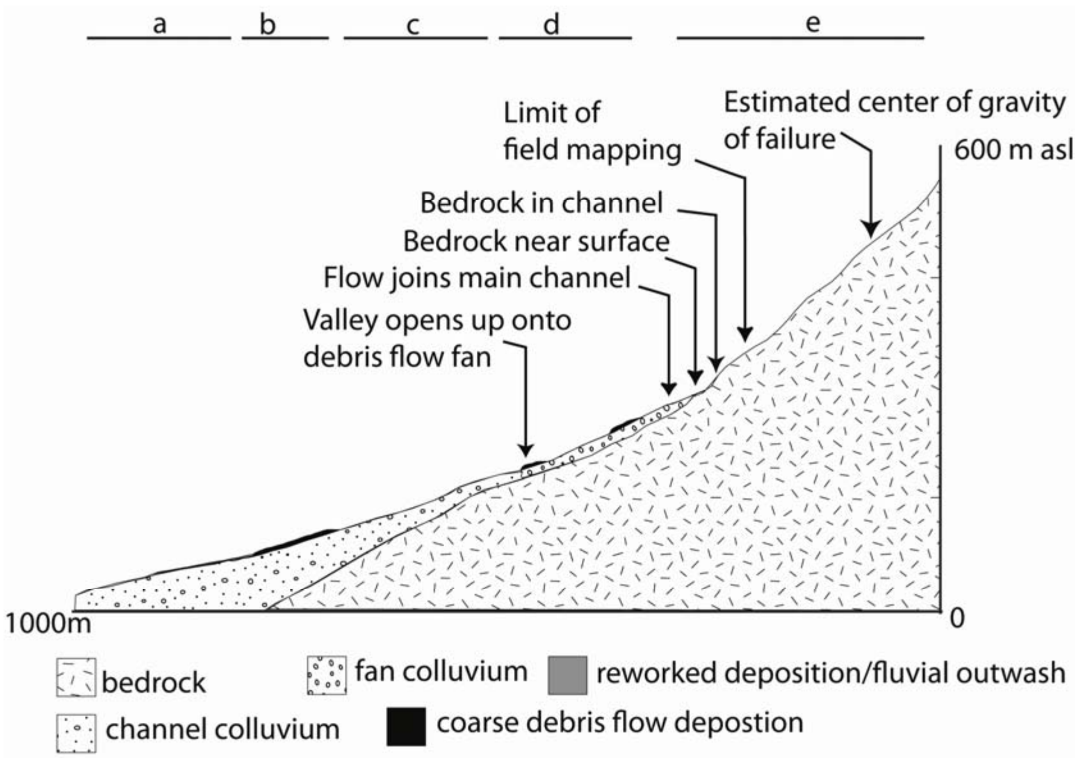

Figure 2 Geomorphic model of OR1. Zone a; reworked deposition and fluvial outwash. Zone b; deposition of coarse colluvium. Zone c; zone of erosion occurring at fanhead. Zone d; transport zone, Zone e; source areas zone..

Figure 3 Particle jamming in OR1

\

Figure 4 Knickpoint in OR1.

Once flows join the main-stem channel, flow behaviour in the upper transport zone is highly unpredictable. While confinement, debris availability, and slope all influence flow behaviour, other factors are important. For example, increased channelization may either encourage erosion, or paradoxically, cause particle jamming at constrictions and encourage deposition, as shown in the photo in Figure 3. These constrictions of large boulders often become knickpoints for subsequent fluvial erosion (Figure 4 Knickpoint in OR1.

The event's kinetic energy (as a function of mass and velocity) upon reaching the fan head maybe another crucial factor in determining entrainment behaviour. In the larger flows (OR1, 3, and 4) the head of the fan was a key area of entrainment. For example, in OR1, this section (Zone (c) in Figure 2) provided the highest yield rates and approximately 40% of all entrainment occurred here. In contrast, for flow OR2 the fan head was a major zone of deposition. It is also possible that channel armouring may limit deposition in some cases. Unlike the rest of the flows in the field area, the source area of OR2 was a lateral talus slope rather than a main bedrock headwall. The maximum particle size deposited on the fan (0.6m in diameter) was noticeably smaller than the undisturbed, 1.0m to 1.5m diameter boulders found in the main channel. It appeared that the combined effect of a larger particle size distribution in the channel from past events of larger magnitude and the removal of fines by stream flow effectively armoured the channel and limited erosion, although this hypothesis needs further investigation.

Once the flows leave the main channel and become unconfined, massive deposition occurs in the form of large lobes of coarse clastic debris (shown as zone (b) in Figure 2). Further downslope, less continuous lenses of finer sediment are deposited by hyperconcentrated or stream flow remobilizing smaller clasts from the main deposition zone. This is referred to as remoulded or reworked deposition in Figure 2. A plan view of OR1 is shown in Figure 5.

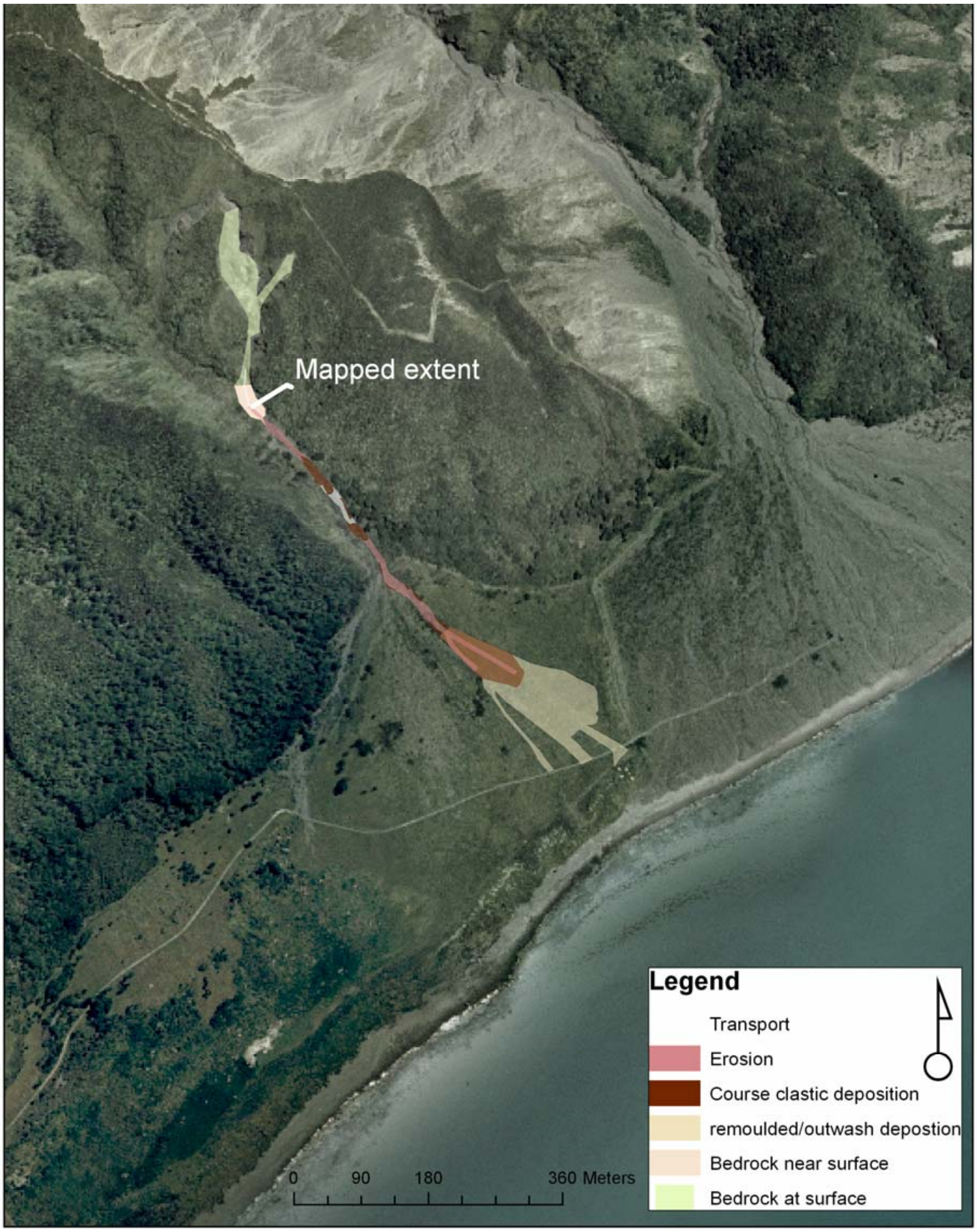

Figure 5 Map view of OR1. Map is developed using…and pasted onto an aerial photograph from…

2.3.2 Cass Field Area

The Cass study area is located on the eastern slopes of the Southern Alps, approximately 20 kilometers east of Arthurs Pass National Park. In April 2009, three flows were investigated, two near the University of Canterbury field station and one on the north side of Purple Hill. Between January and March 2010, three more flows were investigated on Purple Hill, three were added just east of the Broken River near Castle Hill, and two more were mapped near Flock Hill Station off Round Hill (Figure 6).

The bedrock in the Cass study area, as in the Orongorongo study area, is moderate to highly indurated, intricately fractured Triassic sandstone and siltstone, interbedded with minor argillite. However, the most important sediment sources for most of the debris flows mapped are not the bedrock outcrops as in the Orongorongos, but periglacial colluvial deposits mantling the bedrock. Above the bushline, the resulting open talus slopes are one of the most striking features of the eastern Southern Alps and their role in hillslope and landscape evolution has been discussed by several investigators (Whitehouse & McSaveney 1983, Pierson 1982, Hales & Roering 2005). However, no detailed field investigation of these debris flows or gullies has been undertaken since the 1960's (Brundall 1966). According to Brundall, debris flow movement in this area is associated with high antecedent moisture and moderate rainfall, although the precipitation intensity was not unusually high (recurrence interval of two storms per year) for the debris flows that he examined. Based on this data, Brundall suggested that flow triggering is limited by debris accumulation in the channel rather than precipitation intensity.

In contrast to the channelized bouldery type flows observed in the Orongorongos, the slope-type debris flows typical of the Cass study area have received far less attention in the literature (Fannin & Rollerson 1993, Zimmermann 1990, Conway 2009). The flows mapped in Cass are generally smaller, slower, and less hazardous than those in the Orongorongos. Prior accounts of these flows, as well as field observation of a small flow during mapping, show that they travel at no more than a walking pace (Brundall 1966). The highly angular nature of the talus lends these flows a large internal angle of friction. The high friction angle, small peak discharges and possibly lower water content explain the lower velocities.

Unlike the rockfall-triggered flows from the Orongorongos, these flows source from steep, unvegetated talus slopes before entering large gullies at midslope, which generally correspond to the boundary between bedrock near the surface and deeper accumulations of colluvium (see Figure and 8). This area is illustrated by zone (c) in the geomorphic sketch of Cass2 (Figure 9). As the slope angle decreases, the gullies give way to a zone of distinctive natural levees and a U-shaped, luge-like channel (zone (b) in Figure 9). Here, channelization is provided by the natural levees of older flows, with younger deposition inset or mantling older material. This zone can be a major area of deposition, representing nearly 90% of the total depositional volume for Cass1. Deposition of levees and smaller surges may continue for some distance onto the colluvial fan, at which point the levees die out, the flow becomes unconfined, and deposits.

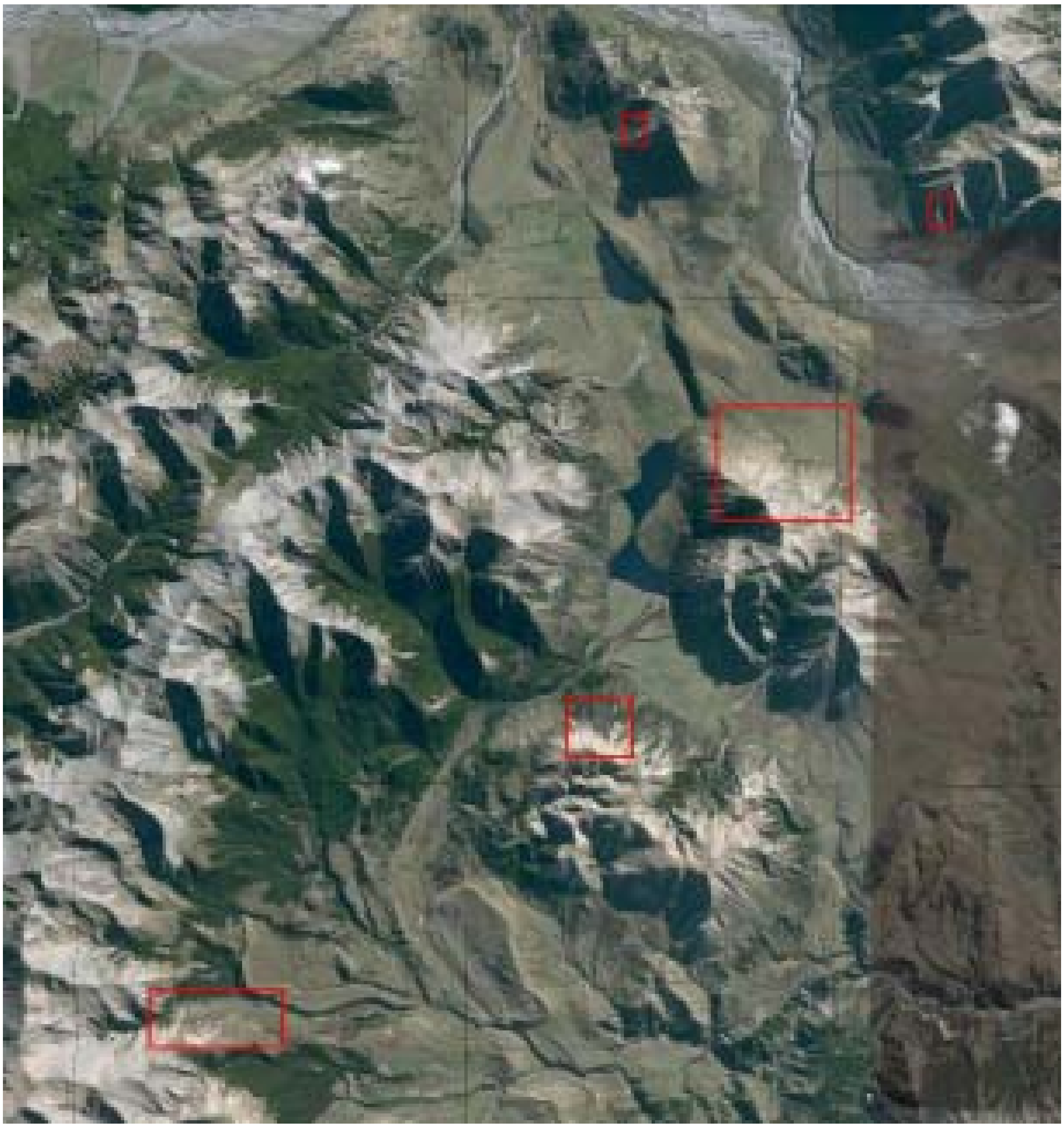

Figure 6 Location of site investigations in the Cass study area. 1. Cass 2, located just southeast of the University of Canterbury field station. 2. Cass 3, located just northwest of Mt. White Road. 3. Cass 3, 6, 7, 11 are located on the north side of Purple Hill. 4. Cass 10 and 12 are located just south of Flock Hill station. 5. Cass 13, 14, and 15 are located just south of Broken stream on Castle Hill station.

Figure 7 Looking down Cass12. Bedrock is within a metre of the surface here, causing the gully to widen rather than incise. The slope angle in this first reach is just at the angle of repose, approximately 38°.

Figure 8 Panoramic view looking down Cass13 and 14. Wide gullying is typical of this upper erosional or transport zone. The flow then transitions into a short section where confinement is provided by natural levees before becoming unconfined on the fan. Terminal lobes of remoulded, reworked material can be seen in the background.

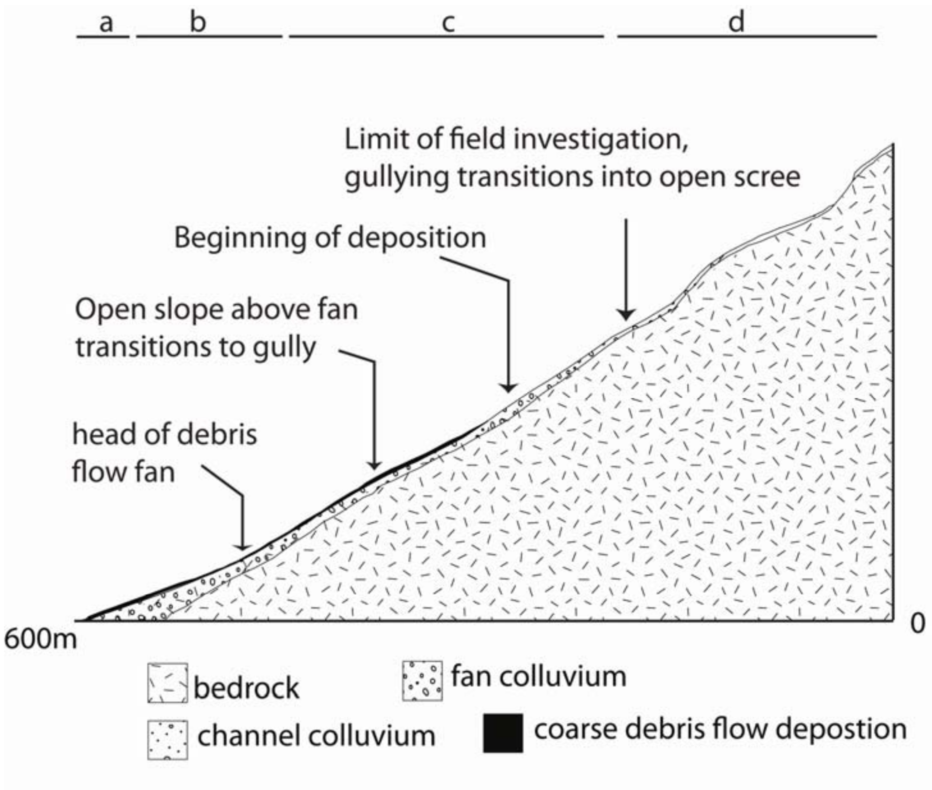

Figure 9 Geomorphic long-section of Cass2. Zone a; Flow becomes unconfined and deposits. Zone b; gully transitions into open slope on colluvial fan, deposition is in the form of levees. Zone c; widening and deepening gully cut into scree slope. Channelization is provided by levees of past flows. Zone d; open scree slope with bedrock at or near the surface.

2.3.3 Birch Hill Field Area

In early February 2010, three debris flows were mapped in the Birch Hill catchment in the Ben Ohau range. This field area is located in Aoraki / Mt. Cook National Park, just east of the main divide. Climatic, geomorphic, and geologic characteristics of this field area differ markedly from those in either the Orongorongos or Cass. While still on the eastern side of the Southern Alps, the field area's proximity to the main divide creates more orographic precipitation when compared to Cass. Annual precipitation values average approximately 4m at Mt. Cook village, several kilometers north of the field area, while values at Cass average only 1m (De Scally and Owens 2003). The bedrock in this area is also more highly metamorphosed, characterized by harder, more intact greywacke to schist with closely to moderately spaced joints.

The mass-wasting processes in the Birch Hill catchment vary more widely than in the Orongorongos or at Cass. Transport by stream flow, debris flow, and snow avalanches are all evident. Most fans and channels are products of all three processes acting in concert (Figure 10).

Flow behaviour in this field area also varies widely, reflecting a transitional form of debris flow between the channelized flows observed in the Orongorongos and the hillslope-style flows observed at Cass. It appears that most of the material in these debris flows are sourced from failures at the boundary of bedrock headwalls and the colluvial foot-slope, although it is possible that rockfalls from higher, inaccessible bedrock reaches may have contributed to the event volumes, especially in flow BH3.

Figure 10: Looking up the Birch Hill Catchment. BH 1, 2, and 3 are seen on the left and source from small rockfalls or translational failures at the bedrock / colluvium boundary. The central channel in the background of the picture is dominantly affected by snow avalanches triggered on Jamieson saddle or Mt. Edgar Thompson headwalls, rather than debris flow processes.

Once triggered, the channel morphology through the transport zone becomes a crucial factor in determining flow behaviour. Debris flows BH1 and 2 are confined for their entire length by an incised gully or natural levees produced from older flows, as shown in Figure 11, reminiscent of the debris flows at Cass. In its upper, source bedrock reaches, BH3 is confined in a bedrock channel and displays evidence of clogging at flow constrictions and knickpoint migration; two processes observed to be important in the Orongorongo field area (see Figure 12).

Figure 11: Looking down BH2. The bank on the true left has undergone considerable trim. Bedrock in the channel and the down-slope limit of the triggering translational failure is visible in the bottom right of the picture.

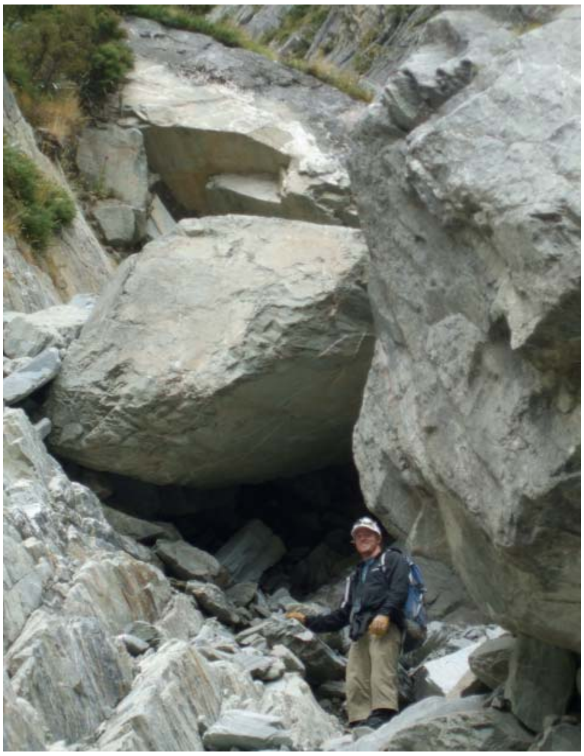

Figure 12: Jamming of large boulders in a bedrock channel in the upper reaches of flow BH3.

The confined flows gradually start depositing in response to lower slope angles. In Cass, the lower threshold for erosive reaches occurs at a slope of approximately 20°, similar to a threshold value of approximately 19° reported by Conway et al (2009) in open-slope type flows in Iceland. Above 20°, deposition occurs sporadically as either lobes or discontinous levees. Below 20°, levees become continuous and massive deposition begins. In BH2, deposition begins to occur at an even higher slope angle, closer to 25°, although in BH3 there are several reaches on shallower slope angles (down to 13°). This probably evinces a higher moisture content or increased fluvial reworking in BH3. In both BH2 and BH3, as in most of the debris flows mapped, a short zone of remoulded or reworked deposition was observed which was created by either the watery tail remobilizing debris from the main deposit or post-event fluvial processes modifying the deposition. This is illustrated in Figure 13, which presents Zone (a) as a short zone of deposition reworked by hyper-concentrated flow and fluvial processes during or post the debris flow event; Zone (b) as a coarse, clastic deposition, either in the form of discreet lobes or continuous lateral levees; Zone (c) as a transport zone with variable erosion and discontinous lateral levees where most erosion is due to marginal trim; Zone (d) in which translational failure occurs near the boundary of bedrock and the colluvial apron and finally, Zone (e) which is bedrock with small, structurally controlled pockets of loose rock.

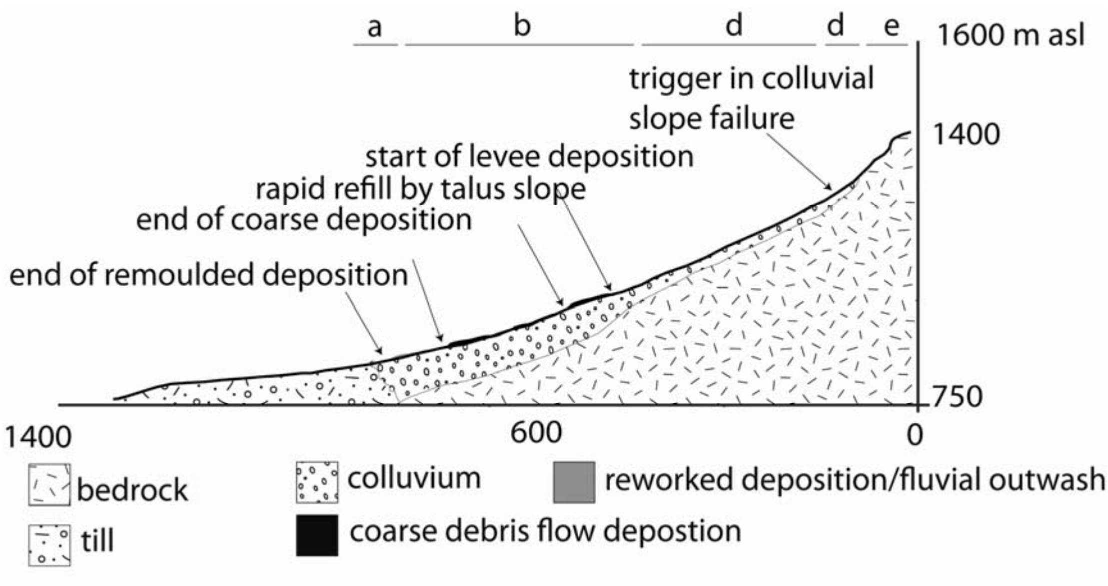

Figure 13: Geomorphic long-section of BH1. Zone a; deposition reworked by hyper-concentrated flow / fluvial processes Zone b; Coarse, clastic deposition. Zone c; Transport zone with variable erosion and levees. Zone d; translational failure. Zone e; bedrock.

2.3.4 Franz Joseph Field Area

In March of 2010, two debris flows were mapped in the Waiho catchment near the Franz Joseph glacier. This field area represents yet another climatic and geomorphic setting for debris flows in New Zealand. The rainfall here is the highest of any of the field areas. The Franz Joseph township recorded nearly 4.6 meters of rain in 2009. The maximum one day rainfall in Franz Joseph during the first week of January, 2010, when the debris flows are thought to have been triggered, was 203mm on January 7th. Maximum hourly rainfall on that day was 36mm. Rainfall values could have been significantly higher in the Waiho catchment.

The bedrock in the Franz Joseph field area consists of moderately jointed chlorite schist, with minor layers of higher metamorphic garnet-bearing schist and lower metamorphic facies. Both of the flows mapped travel down creeks with perennial stream flow before depositing on outwash material from the Franz Joseph glacier and Waiho River.

While large, bedrock waterfalls limited the mappable extent of flows FJ3 and FJ4, lack of mudlines, levee deposition, and lag deposits suggest that debris flow processes were not fully matured in these upper reaches. The flow was probably either clear flood-flow or hyperconcentrated flow here, as the flows had not scoured enough bedrock or colluvium to mobilize into full debris flows.

The major source area for debris in both flows, appeared to be bedrock or colluvial slope failures where flood events had undercut the gully wall. Figure 14 shows a geomorphic long-section of flow FJ4 in which Zone (a) indicates unconfined, coarse clastic deposition; Zone (b) is a deposition zone characterized by continuous levees; Zone (c) is a transport zone with marginal deposition or erosion within a colluvial channel; Zone (d) is a transport zone with bedrock in the channel, limiting erosion to trimming of the colluvial side-walls and Zone (e) is the source zone.

Most debris flow material is sourced from translational failures of channel bank in response to progressive undercutting by flood flow (shown as Zone (e) in Figure 14 and as a photo in Figure 15). This zone was relatively short, only 80m in the case of FJ4 and quickly gave way a transport zone characterized by stochastic erosion and deposition (Figure 16).

In the transport zone, both flows were dominantly confined by the gully. Both debris flow paths displayed auspicious knickpoints formed by large, two to four meter diameter boulders. The quantity of vegetation and organic debris also sets this area apart from others previously studied. In both travel paths, woody vegetation was observed damming the channel and acting as sediment traps. The importance of woody vegetation in mediating channel recharge has been discussed by several authors(Benda and Dunne 1997; Benda and Sias 2003), and there is no reason to doubt this is an important process in the densely forested catchments on the west coast as well.

The channel in both flows remained quite confined until abrupt unconfinement on short, shallow angle fans, at which point the flows deposited. The distal limits of observed fans were often truncated by the Waiho River, which transports debris flow material away during flood events.

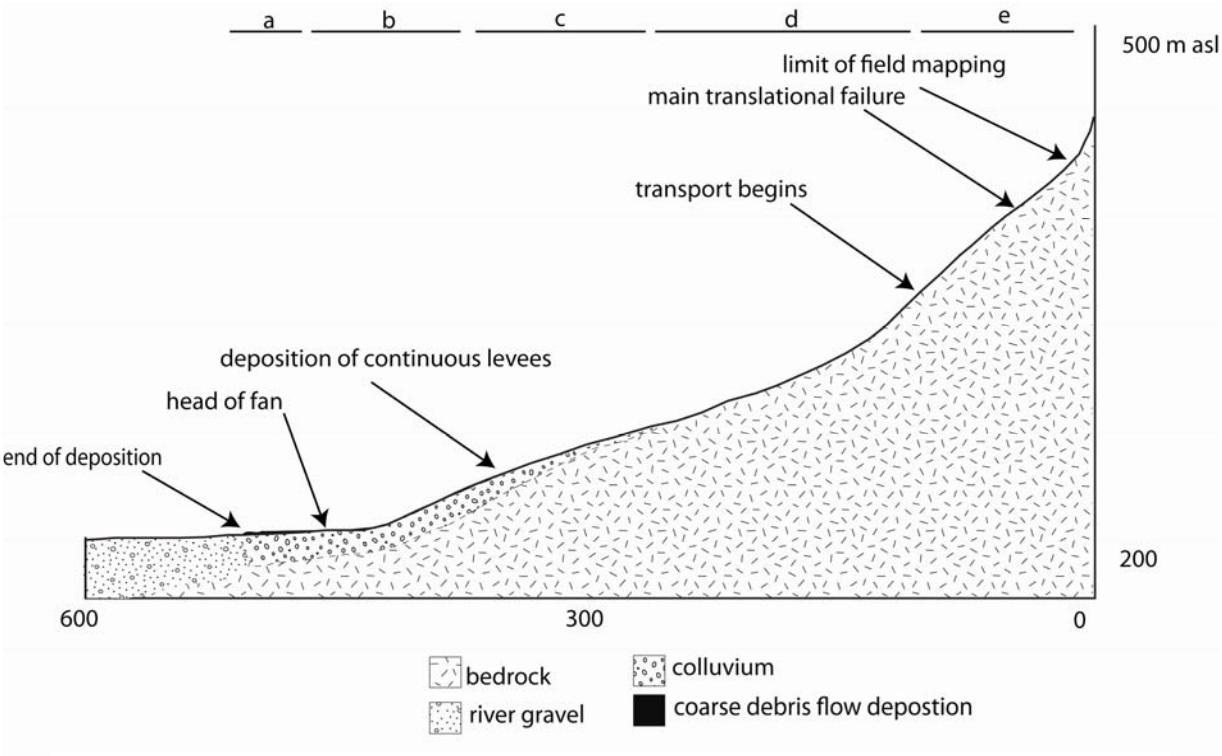

Figure 14: Geomorphic long-section of FJ4. Zone a; unconfined, coarse deposition. Zone b; deposition zone withy continuous levees. Zone c; Transport zone within colluvial channel. Zone d; transport zone with bedrock in channel. Zone e; Source zone.

Figure 15: Upper, source reach of flow FJ4

Figure 16: Transport reach in flow FJ4. Despite leaving a lag of boulders and a lateral levee, the flow has also trimmed the left bank in the photo.

2.4 Discussion and Conclusions

While to this point many of our observations are qualitative, our study is moving us closer to being able to characterize the range of debris flow behaviour in New Zealand alpine catchments, and to connecting these observations back to the underlying mechanics which control that behaviour. Returning back to our initial study questions;

- What types of debris flows are typical of New Zealand alpine catchments?
- How do New Zealand's debris flows compare to other debris flows around the world?
- What empirical models, generated for other localities, are appropriate to use in New Zealand, and in what circumstance?

<u>What types of debris flows are typical of each field area? What are their general characteristics?</u>

Debris flows in the Southern Rimutakas are of the bouldery, channelized type and are most likely triggered by rockfall events in steep, bedrock sources reaches. Volume ranges from 1,000 m^3 to 10,000 m^3 were observed.

Debris flows in Cass are of the slope type, are typically less dangerous, and deposit on high slope angles. Volumes reaching the fan ranged from 100 m^3 to 1,000 m^3, although significant amounts of deposition may occur in natural levees further upslope.

Debris flow behaviour at Mt. Cook is transitional between open, hill-slope type and channelized type and characterized by harder, more metamorphosed rock types than at Cass. Volumes of deposition range from 100 m^3 to 1000 m^3.

Flows near Franz Joseph are of the channelized type, but appear to be characterized by a coarser particle size distribution and more woody vegetation in the depositional material than in other field areas. Volumes of deposition range from approximately 1400 to 2500 m^3.

How do New Zealand's debris flows compare to other debris flows around the world?

Two features make the New Zealand field data set unique. First, the debris flows were mapped in relatively high detail by one lead investigator along with co-workers. Second, the event magnitudes described are relatively small when compared to other debris flows described in the literature.

Figure 17 compares the travel angle and volume relationship for the debris flows investigated in this study with two datasets presented in Rickenmann, 2005. For an adequate comparison, we chose to plot volumes deposited past the last confined reach. This is the volume estimate likely to be reported in most other debris flow studies, as it is the most easily obtained without a detailed field investigation (Rickenmann, pers. communication 2010).

In general, the calculated travel angles shown in Figure 17 are within the variability of debris flows investigated in other areas. However, OR4, Cass1, and Cass10 have anomalous travel angles. In the case of Cass10 and OR4, the solid concentration (i.e. moisture content of the flow) may explain the differences. The lack of any remoulded or fluvial reworked material beyond the main zone of clastic deposition in OR4 suggests that this flow may have been very dry. It also displayed a very wide, steep, and unconfined terminal reach. Consequently, OR4 may be better described as an event transitional between a debris avalanche and the typical channelized, alpine debris flows characteristic of the other three flows mapped in the Orongorongo field area.

Variable fluid content and different fan morphology may explain the anomalously low travel angle of Cass10. Despite the presence of small levees in the upper reaches of this flow, it possible that hyper-concentrated flow, rather than a true debris flow, dominated the upper 9 reaches of this flow. Unlike many of the other flows mapped at Cass, these upper reaches were in a narrow, sinuous, bedrock channel with nearly perennial stream flow and little erosion. Most of the erosion originated from undercutting of gully wall in reaches 10, 11, 12, and 13. In this area, the fan has been incised by up to 16m by stream flow. While evidence of debris flow (i.e. levees) occurred in this zone, the slope of these reaches was relatively gentle (only 12 to 15 degrees) and fluvial processes probably dominated here. In the last three terminal reaches, the slope suddenly steepened and debris flow processes resumed. This morphology also describes Cass 11, although this channel is generally steeper and does not have as much stream flow. Consequently, evidence of debris flow was observed over the entire flow path.

Cass1 and BH1 are also very conspicuous in Figure 17, as they plot below the general trend (i.e. their volumes are lower than expected for their travel angle). Most of the event volume in these events was deposited as lateral levees. These events were also extremely well confined over their length by levees from previous events, which may have increased their mobility. Further, using the unconfined volume past the last confined reach may be less representative with in small, open slope flows, as most of the event volume is deposited as levees.

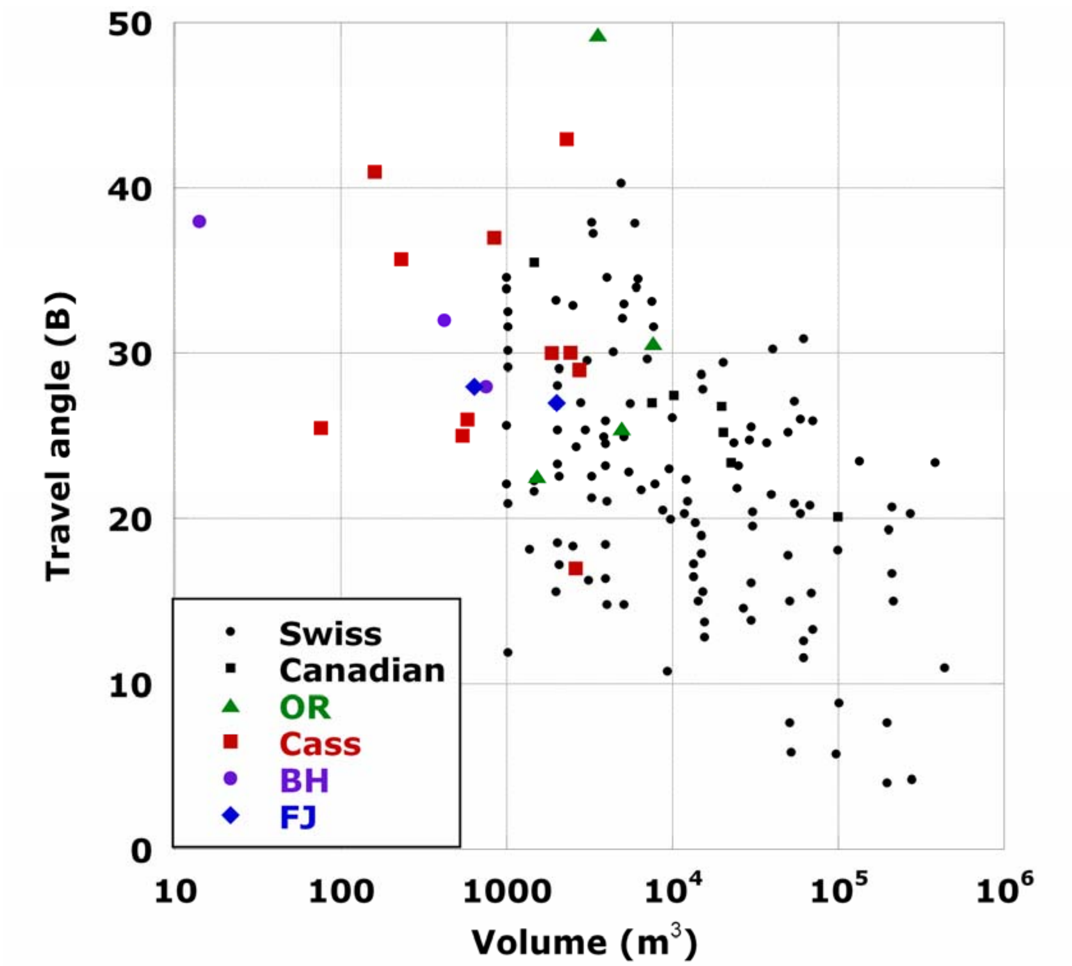

Figure 17: Debris flow travel angle versus volume past the last confined reach.

Figure 17 also shows that the volumes of our data are on the lower end of those reported elsewhere. Most debris flow studies focus on either large, anomalous events or recently disturbed watersheds (i.e. logged or burned terrain). The reasons for this is simple; larger events are usually more destructive, and hence of greater engineering and practical interest, or the study is concerned with informing management decisions about landscape use. However, in depth field investigations of smaller, less-disturbed flows may illustrate limitations on mobility and transport not found in larger, more destructive events. For example, to our knowledge, the effect of particle jamming at flow constrictions or channel armouring has not been observed or studied in the context of debris flows.

Flows of smaller event magnitude also highlight subtle issues regarding confinement. Through the transport reaches of these flows, few of flows mapped were confined by valley sidewalls. Confinement was most often provided a channel cut into the valley fill, or by levees of previous events. The confinement provided by larger, previous events or surges within the same event doubtlessly increases the mobility of later flows. Conversely, some surges that deposited in the transport zone were essentially unconfined in the bottom of the channel. The issue of "relative confinement" is worth considering, as confinement is a key parameter in some empirical models (i.e. Fannin and Wise, 2001). During field investigations over the summer of 2010, relative confinement was accounted for by categorizing reaches as; unconfined in channel, confined in channel (if the flow is essentially bank fall), partially confined by channel, or confined by the gully. Further data analysis will reveal whether these relative confinement categories can be correlated to entrainment and depositional behaviour.

What empirical models, generated for other localities, are appropriate to use in New Zealand, and in what circumstance?

Existing empirical models for channelized type debris flows, such as UBCDFLOW (Fannin and Wise 2001) and ACS (Prochaska 2008) are probably appropriate for preliminary hazard analysis in the Orongorongo and Franz Joseph field areas. The advantage of these two models is that, while empirically-derived from specific datasets in North America, they appear to have a basis in mechanical behaviour. This suggests that it should be possible to transfer most elements of the models to other regions and to make local adjustments only where necessary (e.g. Busslinger, 2010). Some other models (e.g. Rickenmann, 1999; Santi et al , 2001) may require less data input, however they are, as a result limited to the regions from which they are derived, although general comparisons may be useful.

At present, no empirical or analytical models exist specifically for the open-slope type debris flows investigated in Cass and Birch Hill. While these types of flows occur in almost every alpine region worldwide, they have received very little attention in the literature, with the exceptions of studies undertaken in Norway (Conway 2009), and Hong Kong (Fletcher et al 2002, Parry et al 2002).

These field investigations are the first step in systematically characterizing New Zealand's debris flows and developing a national debris flow database and have already started to put New Zealand's debris flows into an international context. They have also produced new, more refined research questions and hypotheses, as well as spawned several other physical modelling studies at the University of Canterbury.

Acknowledgements

This research made possible by the New Zealand Earthquake Commission (EQC) via Bi-annual Grant BIE 08-548 and a University of Canterbury Doctoral Scholarship. Field assistance was provided by Sam McColl, Warren McKenzie, Susan Neuner, and Angus Newsam. Thanks also to Chris Massey of GNS Science for his time and help in the field.

REFERENCES

Begg, J. G., & McSaveney, M. J. 2005. Wairarapa fault rupture and vertical deformation in 1855 and a history of similar events from Turakirae Head. Paper presented at the 1855 Wairarapa Earthquake Symposium.

Benda, L. and T. Dunne 1997. Stochastic forcing of sediment supply to channel networks from landsliding and debris flow. *Water Resources Research* 33(12): 2849-2863.

Benda, L. and J. Sias 2003. A quantitative framework for evaluating the mass balance of in-stream organic debris." *Forest Ecology and Management* 172(1): 1-16.

Brundall, J. A. 1966. Recent debris flows and related gullies in the Cass Basin. University of Canterbury, Christchurch.

Busslinger, M. 2010. Empirical Rules for Debris Flow Travel Distance: A Comparison of Field Data. Civil Engineering. Vancouver, The University of British Columbia. M.Sc.: 152.

Conway, S. J., Decaulne, A., Balme, M. R., Murray, J. B., & Towner, M. C. 2009. A new approach to estimating hazard posed by debris flows in the Westfjords of Iceland. *Geomorphology*.

Fannin, R. J., & Rollerson, T. P. 1993. Debris flows: some physical characteristics and behaviour. *Canadian Geotechnical Journal CGJOAH*, *30*(1), 71-81.

Fannin, R. and M. Wise 2001 An empirical-statistical model for debris flow travel distance. *Canadian Geotechnical Journal* 38(5): 982-994.

Gartner, J. E., Cannon, S. H., Santi, P. M., & Dewolfe, V. G. 2008. Empirical models to predict the volumes of debris flows generated by recently burned basins in the western US. *Geomorphology*, *96*(3-4), 339-354.

Hales, T. C., & Roering, J. J. 2005. Climate-controlled variations in scree production, Southern Alps, New Zealand. *Geology*, *33*(9), 701.

Hungr, O. 1995 A model for the runout analysis of rapid flow slides, debris flows, and avalanches. *Canadian Geotechnical Journal* 32(4): 610-623.

Hungr, O., Evans, S. G., Bovis, M. J., & Hutchinson, J. N. 2001. A review of the classification of landslides of the flow type. *Environmental and Engineering Geoscience*, *7*(3), 221.

Hungr, O., McDougall, S., & Bovis, M. 2005. Entrainment of material by debris flows. In M. Jakob & O. Hungr (1st Ed), *Debris-flow Hazards and Related Phenomena.* Springer-Praxis: New York.

Jakob, M. 2005. A size classification for debris flows. *Engineering Geology*, *79*(3-4), 151-161.

McSaveney, M. J., Beetham, R. D., & G.S., L. 2006. The 18 May 2005 debris flow disaster at Matata: Causes and mitigation suggestions.

McSaveney, M. J., & Davies, T. R. H. 2005. Engineering for debris flows in New Zealand. In M. Jakob & O. Hungr (1st Eds), *Debris-flow Hazards and Related Phenomena.* Springer-Praxis: New York.

McSaveney, M. J., & Glassey, P. J. The Fatal Cleft Peak Debris Flow of 3 January, 2002, Upper Rees Valley, West Otago, 28.

Pierson, T. C. 1982. Classification and hydrological characteristics of scree slope deposits in the Northern Craigieburn Range, New Zealand. *Journal of Hydrology (NZ)*, *21*(no. 1), 34-59.

Prochaska, A., P. Santi, et al. 2008. Debris-flow runout predictions based on the average channel slope (ACS). *Engineering Geology* 98(1-2): 29-40.

Rickenmann, D. 1999. Empirical Relationships for Debris Flows. *Natural Hazards*, *19*(1), 47-77.

Rickenmann, D. 2005. Runout prediction methods. In M. Jakob & O. Hungr (1st Ed), *Debris-flow Hazards and Related Phenomena.* Springer-Praxis: New York.

Santi, P. M., dewolfe, V. G., Higgins, J. D., Cannon, S. H., & Gartner, J. E. 2008. Sources of debris flow material in burned areas. *Geomorphology*, *96*(3-4), 310-321.

Welsh, A. J. 2007 Delineating debris flow hazards on alluvial fans in the Coromandel and Kaimai regions, New Zealand, using GIS, University of Canterbury. MSc.

Whitehouse, I. E., & McSaveney, M. J. 1983. Diachronous talus surfaces in the Southern Alps, New Zealand, and their implications to talus accumulation. *Arctic and alpine research*, *15*(1), 53-64.

Zimmermann, M. 1990. Debris flows 1987 in Switzerland: geomorphological and meteorological aspects. *IAHS, Hydrol. Mountainous Regions*, *2*(194), 387-393.

CHAPTER 3: PHYSICAL MODELLING OF DEBRIS FLOWS ON THE CENTRIFUGE

ABSTRACT

This chapter describes a series of experiments on debris flows, using a small-scale flume housed within a geotechnical centrifuge. The experiments were designed to examine the effect of varying the moisture content (or solid concentration) and flow volume on debris flow velocity, discharge, and runout. The effect of pore-fluid rheology was also examined by using both Newtonian and non-Newtonian pore fluids. As expected, an increase in flow volume and in moisture content was found to increase the peak velocity of the flow during down-slope movement, regardless of which pore fluid was used. The influence of increased moisture content on peak velocity was found to be much more pronounced than that of increased bulk volume.

The cross-sectional area of the flow was governed in these tests by the flow height, since the flow channel was rectangular. The maximum cross-sectional area of flow (or maximum flow height) observed was found to be independent of both total flow volume and moisture content and was likely limited by the flow rate entering the head of the flume. Consequently, the flow velocity largely determined the peak discharge of each flow. An increase in moisture content increased the mobility of the flow, in terms of velocity and also in terms of inundated depositional area and runout.

Once unconfined, the runout, measured as the distance of the centre of mass of deposits from the flume outlet, was compared against several measures of the flow, including the square of velocity, the flow volume and the peak flow momentum. A linear relationship was observed between flow volume and runout and also between the square of velocity and runout for flows (albeit with a greater degree of scatter) at a given moisture content, however, these relationships changed with the moisture content. The runout was also found to be linearly related to the peak momentum of the flow near the flume outlet – in this case, however, flows of both different moisture content and volume appeared to lie on the same trendline, while a single test using an erodible bed also plotted on this line.

These relationships were found to hold for flows carried out with both pore fluids, however, velocity and runout behaviour differed between tests carried out with different pore fluids. In the channel, the non-Newtonian flows accelerated and decelerated much faster than the Newtonian flows. However, based on the momentum of each flow at the camera frame, the non-Newtonian flows showed less runout than an equivalent test carried out using a Newtonian pore fluid. In theory, the range of global shear rates, determined as the ratio of surface velocity to flow height, experienced by the non-Newtonian flows, should not have led to great changes in

viscosity during tests conducted with this fluid. However, the marked difference in behaviour between tests using Newtonian or non-Newtonian fluids shows the viscosity to be changing dramatically with the non-Newtonian fluid. This suggests that global shear rates may not be as relevant as local intergranular shear rates in developing the fluid rheology. These results may help to shed light on the role of different interstitial fluids such as water and mud on debris flow behaviour. It appears that the introduction of a non-Newtonian pseudo-plastic fluid, such as mud, can result in a form of feedback, so that faster flow during downslope acceleration results in a drop in viscosity, leading to greater acceleration. However, this may not translate to longer runout overall, since as the slope reduces and the material slows, the feedback operates to decelerate the flow, increasing the viscosity and further reducing the flow momentum.

2.1 Introduction

2.1.1 Physical modelling of debris flows

The highly complex, stochastic nature of debris flows is a direct result of the synergistic interaction between their fluid and solid phases. Key debris flow parameters such as particle size distribution, moisture content (as used in soil mechanics) or solid concentration (as used in fluid mechanics), velocity, and discharge vary spatially and temporally as a debris flow travels down its path. This makes understanding and modelling the mechanics of debris flow motion difficult. Even if one is lucky (or unlucky) enough to be able to observe a debris flow event in the field, the boundary conditions and key parameters influencing flow behaviour may be difficult or even impossible to measure.

Physical modelling simplifies these processes and allows boundary conditions to be controlled from the comfort of the lab, without preconditioning the outcome. This has made small-scale flume studies of debris flows an indispensable tool in elucidating the key aspects of debris flow mechanics. However, there are some drawbacks to flume studies at the small scale. The extrapolation of small-scale behaviour to field scale processes may not always be appropriate, as small scale flows may not reflect the dominance of Coulomb stresses and decreasing importance of viscous stresses in field scale flows (Iverson and Denlinger 2001). Modelling of flows in a geotechnical centrifuge overcomes some of these limitations by increasing the g-level, which increases prototype stress levels while preserving the convenience and flexibility of the small scale flume modelling. Previous work has demonstrated the ability of the geotechnical centrifuge to model flows at more appropriate stress levels (i.e. in a more frictional regime) (Bowman et al. 2007; Bowman et al. 2010; Bowman et al. 2006).

2.1.2 Volume, moisture content and velocity effects

The aim of the experiments presented in this report was to extend the aforementioned work by investigating the influence of flow volume and moisture content (or solid concentration) on debris flow behaviour in the centrifuge, as measured by flow velocity, flow depth, discharge and runout.

Debris flow volume is often cited as the most critical parameter in estimating debris flow hazard, as larger flows travel faster and farther than smaller flows, both at the lab and field scale (Hungr et al. 1984a; Jakob 2005; Rickenmann 1999; Rickenmann 2005). Further, previous work has shown that the peak discharge of the flow can be related to the debris flow volume (Rickenmann 1999). However, moisture content may be just as important, if not more important, than event volume in some cases. For example, in field and laboratory investigations of runout distances in Dolomites, moisture content was found to control runout almost regardless of event volume (D'Agostino et al. 2010). Takahashi (2007) discusses the importance of grain concentration, which decreases with increasing moisture content, in controlling the velocity distribution of particles with depth. That is, the greater the moisture content, the less the frictional contact between particles, and the lower the resistance to flow. Thus, the moisture content has a profound influence on shear rate, peak discharge, and peak velocities (which in turn affect impact pressures on any structures or natural materials in the path of the flow, and which may also be entrained into it).

2.1.3 Pore fluid effects

As discussed further below, in centrifuge testing of diffusion processes (such as experienced in a debris flow), it may be necessary to increase the pore fluid viscosity in order to correctly scale diffusional and inertial times in the model. For the tests described here, this presented an opportunity to examine the influence of fluid rheology on the modelled debris flows, by comparing a Newtonian fluid with a non-Newtonian fluid. Hence, several experiments were repeated using the same quantity of dry materials and fluid, while altering the pore fluid rheology. We used methyl cellulose (mc) as the non-Newtonian pore fluid and glycerine (gl) as the Newtonian pore fluid.

While specifying rheological parameters is critical for many analytical models for debris flow runout, the appropriate values to use is often difficult to determine, even in the lab. For example, the effective viscosity of a flow may change with even small changes in particle size distribution and shear rate (Phillips and Davies 1991). Given the fact that the particle size distribution and moisture content of a flow is temporally and spatially variable, some investigators have even questioned the appropriateness of trying to characterize a flow with one rheological model (Iverson 2003). The intent in comparing the influences of a non-Newtonian versus a Newtonian pore fluid was not to model the behaviour of specific field scale flows, which always have a pore fluid of water and suspended fines and which subsequently display a variety of apparent rheologies, but to isolate the effects of the pore fluid behaviour on debris flow velocity and runout. Results are later discussed in this context.

2.2 geotechnical centrifuge tests

2.2.1 Concept

Geotechnical centrifuge testing enables an exploration of the aforementioned and other variables under controlled boundary conditions and to run tests at stress-levels that are more appropriate to typical prototype field events than provided by conventional flume tests. At the same time, centrifuge testing allows more detailed observation than possible at the field scale. This technique also enhances the flexibility and novelty of conventional flume testing, since the effective g-level experienced by the model can be manipulated. The principles of centrifuge testing as applied to debris flow research are discussed briefly below. Further information can be found in Bowman et al (2010).

2.2.2 Programme

The preliminary results from nine debris flow tests are presented in this chapter. Using glycerine as the pore fluid, three tests were run with different volumes of material (by mass of dry solids: 1 kg, 1.75 kg, and 2.5 kg) with a moisture content of 33% by mass, while a last test was run using 1.75 kg of dry solids with a moisture content of 39% to investigate the influence of increased moisture content.

Similarly, using methyl cellulose as the pore fluid, three tests were performed using 1 kg, 1.75 kg, and 2.5 kg of dry material. A fourth test was conducted at a higher moisture content (36%), while a fifth test was run using 2.5 kg of flow over a 1.5 kg (dry mass) erodible bed prepared at 15% moisture content.

Table 1 gives details of each of the tests, with a detailed test code for each. Note that throughout the report, the tests are referred to by a shortened version of the test code: i.e. test T7_V_MC becomes test T7.

Table 1 Test code and a short description of the bed type, pore fluid used, amount of solid material used, and the moisture content of each flow. Moisture content is defined as ($Mass_{liquid}/Mass_{solid}$) as a percentage. The viscosity of the glycerine pore fluid was 42cP at 20ºC. The viscosity of the methyl cellulose was approximately 45cP at a shear rate of $10s^{-1}$ and decreased with increasing shear rate.

Test Code	**Bed**	**Pore fluid**	**Mass dry solids (kg)**	**Moisture content (%)**
T7_V_MC	Fixed	methyl cellulose	2.5	33
T9_V_MC	Fixed	methyl cellulose	1	33
T10_V_MC	Fixed	methyl cellulose	1.75	33
T12_W_MC	Fixed	methyl cellulose	1.75	36
T17_E	Erodible	methyl cellulose	2.5: flow, 1.5: bed	33: flow, 15: bed
T14_V_G	Fixed	glycerine	1.75	33
T15_V_G	Fixed	glycerine	1	33
T20_V_G	Fixed	glycerine	2.5	33
T23_W_G	Fixed	glycerine	1.75	39

2.3 Centrifuge testing

2.3.1 Apparatus and instrumentation

Details regarding the design and instrumentation used in the experiments have been discussed previously (Bowman et al. 2007; Bowman et al. 2006; Springman et al. 2001a). However, a brief description of the apparatus and some minor changes to the flume relevant to the proceeding discussion is given below.

Experiments were carried out using the ETH Zurich Geotechnical Drum Centrifuge in Switzerland. This centrifuge has a maximum working radius of 1.1m, a maximum design acceleration of 440g, and a maximum load carrying capacity of 2000kg (Springman et al. 2001b).

The debris flow apparatus was designed to guide liquefied debris flow material from its head to the inner circumference of the centrifuge drum. The drum circumference itself was used as the runout zone – i.e. where the flow comes to rest. Several holes located along the circumference of the drum allowed fluid to be removed from the consolidating debris flow deposit to be collected outside the rotating parts of the centrifuge.

The debris flow flume apparatus consisted of a channel, a strut and a curved support to spread load to the drum. The 600mm long flume was curved to follow the inner curvature of the drum, such that, at a slope angle of 0°, it would lie evenly along the drum circumference (Figure 1). The flume width in this round of tests was decreased from 160mm, as used in previous tests, to 60mm to provide increased channelization and hence increased flow velocity towards values more representative of field scale flows than those obtained previously. The greater degree of channelization also increased flow depth, which, when combined with a coarser particle distribution, enabled individual particles to be tracked in the fast camera images.

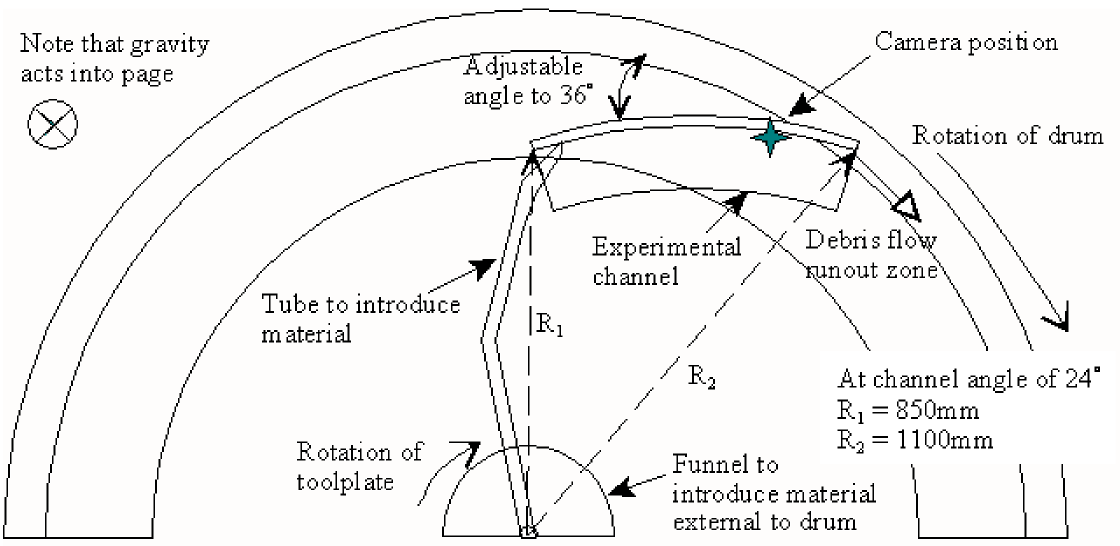

Figure 1 Plan cut-away schematic view of the debris flow channel within the drum centrifuge (only half of the drum shown)

Six pore pressure transducers (PPTs) were provided along the base of the flume for the measurement of pore pressure during the experimental debris flows. Coarse sand particles glued to the base provided a rough substrate; the smooth aluminium and Perspex walls ensured relatively plane strain behaviour.

The upper Perspex side of the channel allowed a small monochrome high-speed digital camera (500fps at full scale of 240 × 240 pixel) to observe an elevation view of the flow during the test. Small markers were painted on the window to enable tracking of the flow. The flow was lit by a close array of 8 LEDs embedded in the Perspex window. The camera was started by the cutting of a light barrier at the head of the flume, as the flow front passed.

The unconsolidated debris flow material was introduced "in flight" to the channel by a flexible feeder tube. The tube extended from the central axis of the centrifuge, where material was delivered via a funnel, and was guided by an actuator on the centrifuge tool plate to the head of the channel, where it exited to flow outward under centrifugal acceleration, down the slope. This system enabled the material to be prepared and maintained as a slurry external to the drum (in which it would otherwise consolidate during spin-up).

After each test, measurements were taken of the maximum runout and lateral spread of each flow. In addition, reference marks running vertically and horizontally on the drum surface were used as a grid to record spot depths of the flow deposition (Figure 2). This data was then used to compare the morphology of deposition and runout.

Figure 2 Deposition from T15 which has consolidated on the drum surface after spin-down. The markers in seen act as reference points for point measurements of depth.

2.3.2 Centrifuge scaling principles

Due to the effects of stress level, flow thickness and permeability, small-scale geotechnical models tested at Earth's gravity are not generally adequate for simulating particular aspects of debris flows, such as erosion, and for examining scaling laws. Geotechnical centrifuge modelling involves testing a soil model of 1/N scale under a centrifugal acceleration of N times Earth's gravity – i.e. N×g. This offers the possibility to examine debris flow processes by modelling at stresses that approximate prototype values and by the careful selection of materials to replicate correct diffusional and inertial times.

Scaling principles have been developed for the geotechnical centrifuge over a number of years for both static and dynamic processes including seismically induced liquefaction, rockfall behaviour, fluid flow and erosion (Chikatamarla et al. 2006; Craig et al. 1988; Garnier et al. 2007; Schofield 1980). Debris flows are a relatively new phenomenon to be tested on a centrifuge; however, it is generally accepted that within a debris flow, the flow will be laminar as a result of the high concentration of particles and small particle size (Hungr et al. 1984b; Iverson 2005). Laminar flow scaling follows Darcian / conventional consolidation laws (Goodings, 1982), hence these principales have been followed in the centrifuge scaling applied.

Scaling relationships for geotechnical centrifuge modelling are shown in Table 2 (Steedman and Zeng 1995). Note that for dynamic processes involving laminar flow, inertial effects (which scale to 1/N) and diffusional effects (which scale to $1/N^2$) scale differently over the same time period. To resolve this inconsistency, the prototype pore fluid (assumed to be water) is replaced with a higher viscosity pore fluid which inhibits consolidation (Kutter 1995). If the viscosity of the pore fluid is N times higher than water, it slows down the time for consolidation by N^2 and inertia by N in the model, resulting in the same overall time for these processes as the prototype with water. This approach also means that the particle size distribution, PSD, used in the model is the same as the "effective" PSD at the prototype scale. To match time-scales here, glycerine and methyl cellulose pore fluids were used as alternatives in different tests; the advantages and disadvantages of each will be discussed later.

In all tests described here, an acceleration factor N = 40 was used (i.e. the effective acceleration was N times Earth's gravity g). As a result, the viscosity of the pore fluid was designed to be approximately 40cP for the flow conditions, as discussed further below. The mass of material used at the prototype scale in the tests was varied from 1 kg to 2.5 kg, which experiences, at N = 40, the static stresses felt by 40 kg to 100 kg of the material at the prototype scale. For N = 40, the prototype channel dimensions scale to 28m long by 2.4m wide. Peak flow heights were recorded at between 10 and 17 mm high, corresponding to a prototype flow height of 400 to 680 mm.

While the prototype length scales and effective PSD come close to replicating some small, field-scale debris flows, this prototype was not chosen to replicate any particular event. The prototype should still be considered highly idealized.

Table 2 Scaling laws used in geotechnical centrifuge testing, based on $N\times g = r\times\omega^2$, where ω is angular velocity.

Parameter	Prototype (field)	Model (centrifuge)
Gravity acceleration	g	Ng
Stress	σ	σ
Displacement / length	x	x/N
Velocity	v	v
Acceleration	a	aN
Time (inertial)	t_i	t_i/N
Frequency	f	f
Time (diffusional)	t_d	t_d/N^2
Energy	E	E/N^3

2.3.3 Pore fluid

As mentioned above, two pore fluids were used to achieve a match between inertial and diffusional time scales; a solution of water and glycerine (gl) and water and methyl cellulose (mc). Each has advantages and disadvantages. Using both pore fluid types for tests in which other variables were kept the same enabled each fluid to be evaluated from a practical, experimental perspective. It also allowed the manipulation of a variable not often tested in conventional flume studies.

A solution of glycerine and water is Newtonian, meaning its stress versus strain rate curve is linear, making it a convenient pore-fluid in many geotechnical applications where viscosity needs to be controlled. However, it is also hygroscopic, attracting water molecules to it from the atmosphere, and it cannot be fully dehydrated once mixed with water. This prevents any determination of moisture contents or sieve analysis after the test, since the mixture cannot be completely oven dried.

Methyl cellulose has an advantage over glycerine in tests in which knowing the particle size distribution or moisture content is important at the test end, since it is not hygroscopic and dries to a fine powder at 100°C, allowing the fluid to evaporate and solid materials to be sieved out. However, non-Newtonian methyl cellulose is also pseudo-plastic or “shear-thinning”, meaning that the viscosity decreases with increasing shear rate. This means that the effective viscosity decreases, and hence the rate of consolidation of the flow increases with increasing shear rate. Figure 3 shows the viscosity versus shear rate of both methyl cellulose and glycerine fluids, measured by viscometer, as well as the range of globally determined shear rates encountered in the tests. The specific form of methyl cellulose chosen was designed to develop as constant a viscosity as possible over the working range of global shear rate, however, note that over the range of shear rate encountered in the tests, the viscosity may drop by approximately 1/3.

The use of a non-Newtonian pore fluid may not reflect all field debris flow conditions (i.e. for typical stony or granular debris flows), however, in this case that is not the intention. Isolating the pore fluid as a variable has the potential to elucidate aspects of the interaction between the solid and fluid phases of the flow. For example, it may possible to assess the dominance of particular mechanisms such as viscous shearing over diffusion within the downslope and runout motion of debris flows; interactive mechanisms that hitherto have not been able to be separated.

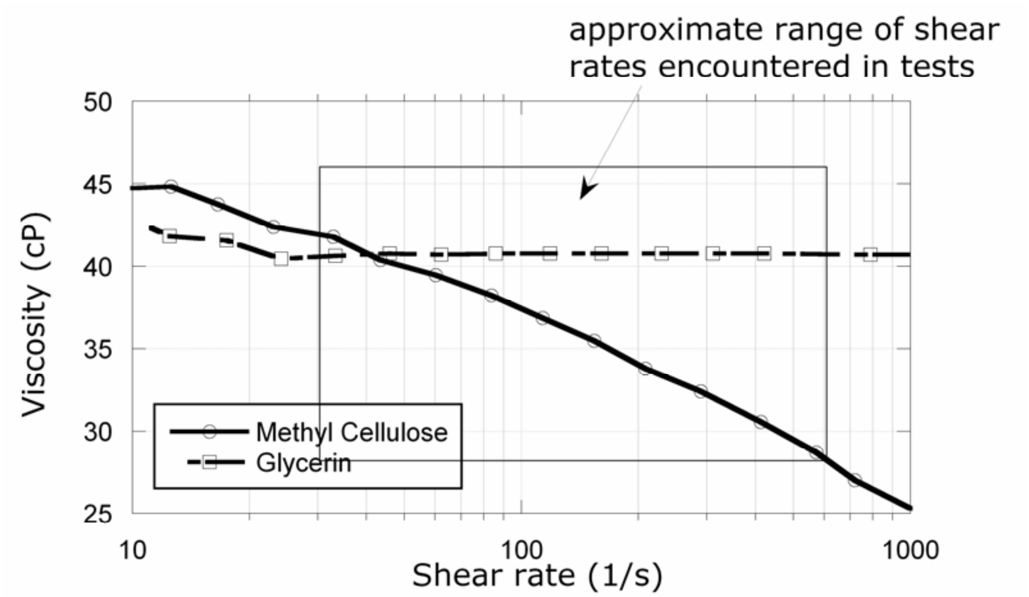

Figure 3 Effective viscosity data for glycerine and methyl cellulose. The range of maximum global shear rates for the tests is also shown.

Finally, it should be noted that the use of either a Newtonian or a pseudo-plastic pore fluid within a model may be dictated by modelling a specific debris flow type. Granular debris flows tend to have low quantities of fines in the form of clay and silt (< 5% by mass, (Takahashi, 2007)), hence such flows are generally modelled as Newtonian and frictional. Conversely, muddy debris flows (Takahashi, 1991; 2007) tend to have their coarser clasts mixed within muddy suspensions. Such suspensions and hence the flows generated in these materials are often modelled as Bingham fluids (exhibiting a linear shear resistance-shear rate relationship after an initial yield shear stress has been reached). However, since mud suspensions are in general pseudo-plastic, this is actually a simplification and it may be more appropriate to use a truly pseudo-plastic material and model the fluid behaviour as such.

2.3.4 Material constraints

Experimental constraints limit the particle size distribution tested in the centrifuge. The maximum size particle used is limited by the narrowest internal point of constriction in the feeder tube (where the internal diameter is 32mm). The maximum particle diameter is approximately 4mm (Bowman et al. 2006). Particles larger than this can cause mechanical arching and flow blockage. The particle size distribution tested represents a compromise between the largest D90 (2mm) possible, while still allowing a relatively high value of Cu (d_{60}/d_{10}) of 36.7, which is shown to be an important parameter in other physical modelling studies of debris flow behaviour (Bowman and Sanvitale 2009).

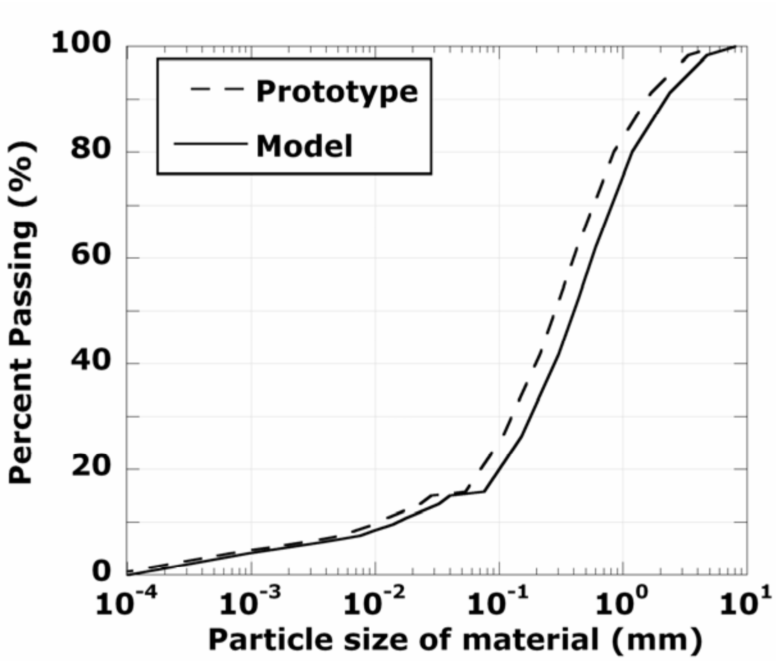

Figure 4 Real and effective PSD used in all tests, assuming a viscosity of 42cP (42 times the viscosity of water).

The material used in these tests was a mixture of soil from three separate localities, two in New Zealand and one in Switzerland. The largest fraction used (approximately 48% by weight) was collected from the Mt. Thomas debris flow site in Northern Canterbury. This locality has been a site of ongoing debris flow activity since 1977, when a series of debris flows were triggered on recently harvested cut blocks (Pierson 1980). The material from Mt. Thomas was supplemented in the range of 0.6mm to 0.075mm with fluvial material available at ETH, since sieving out enough sand and silt strictly from the Mt. Thomas material was impractical. 41% of the PSD tested was made from this fluvial material. The lighter colour of this sand also created slightly more texture in the fast camera imagery, which was useful for post-processing. The last and generally finest 11% of the mixture came from Loess collected from slips in the central north island of New Zealand. This provided the remainder of the fine sand, silt, and clay in the particle size distribution used in the tests, as shown in Figure 4. Atterberg limit tests were carried out on both Mt Thomas and North Island Loess materials (percentage passing 75µm). These generally showed that the fines were non-plastic and hence, applicable to stoney or granular debris flows (Takahashi, 1991) – see Table 3 for details.

Table 3 Soil plasticity parameters for the fines used in the experiments

Soil type	**Liquid limit, w_{LL} (%)**	**Plastic limit, w_{PL} (%)**	**Plasticity Index, PI (%)**	**Classification**
Mt Thomas	33.7	23.3	10.4	Non-plastic silt
North Island Loess	30.1	22.2	7.9	Low plasticity clay

2.4 Test results

2.4.1 High speed camera imagery and flow heights

The high speed camera was placed to give a side-wall view of the debris flow as it passed the Perspex window. Images were taken at 333 frames per second (fps) for up to 18 seconds. In every flow, a fast, coarse, unconfined flow front of high solid concentration preceded the peak discharge, as shown in Figure 5.

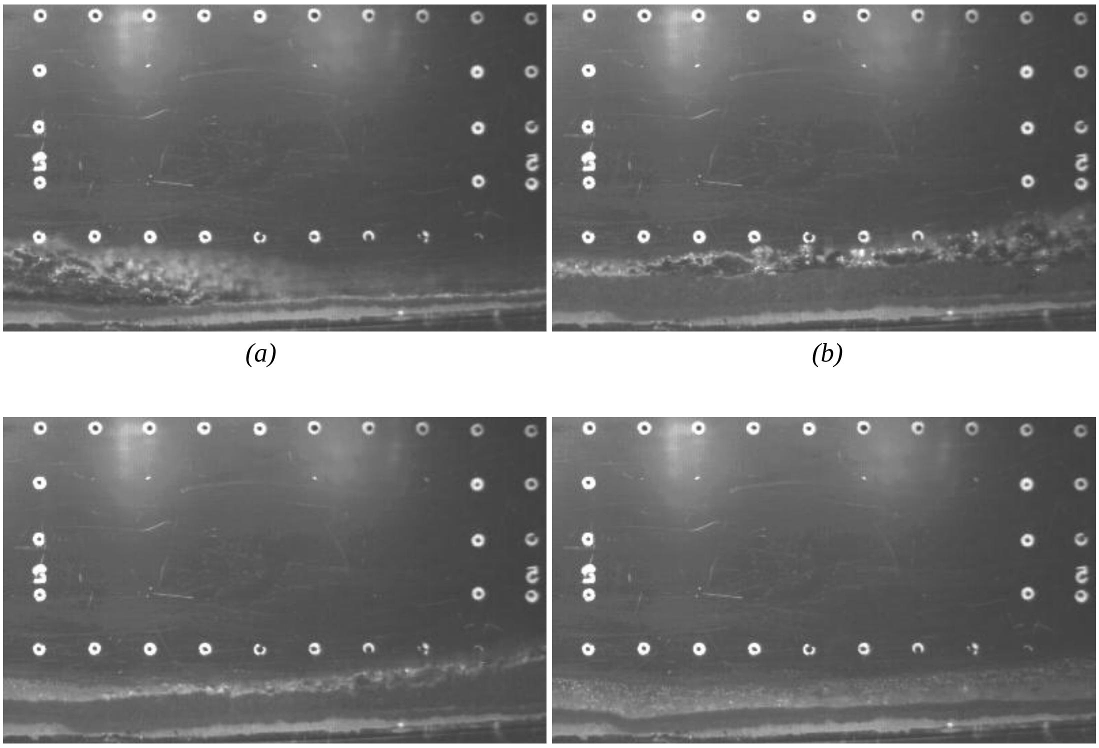

(a) *(b)*

(c) *(d)*

Figure 5 Fast camera imagery from T14, frames (a) 644, (b) 707, (c)769, (d) 1501. Flow proceeds right to left, the dot spacing is 10mm. The sequence shows (a) the arrival of the front, (b) thickening of the front,(c) thinning of the front and (d) transition to the watery tail portion of the flow.

The surface of each flow was nearly always slightly higher in the middle than on the edges due to the parabolic shape of the free surface. While particles up against the Perspex window were in focus, because of the limited depth of field set by the camera focus and aperture to give the greatest light input, particles near the centre were somewhat blurry and indistinct. This can be quite clearly seen in Figure 5. To explore the flow depth change over time, the flow height at the free surface and against the window over a series of frames, were measured. The measurements were taken at least every four frames during front passage, then every several hundred frames in the watery tail portion of the flow when the rate of change dropped significantly. From this data, a cross-sectional area of the flow for each frame could be calculated.

In all the tests, the depth of flow abruptly increased, rapidly attenuated, and then slowly decreased in accordance with a near-power law (an example from the 1 kg glycerine test, T15, is shown in Figure 6, with the best-fit power law for this case). The inflection point in the flow depth and discharge plots roughly coincided with the point where coarse particles located on the surface of the flow were much less visible in the fast-camera imagery, reflecting the transition to the "watery tail" portion of the flow (Figure 10 and 12).

Images from the high-speed camera also enabled the change in surface velocity of the flow over time to be determined. By tracking individual particles over several frames (as many frames as each particle was distinguishable), an instantaneous velocity of the particle was calculated for portions of the flow. This velocity data was used to construct the debris flow hydrographs and velocity profiles discussed later in the chapter.

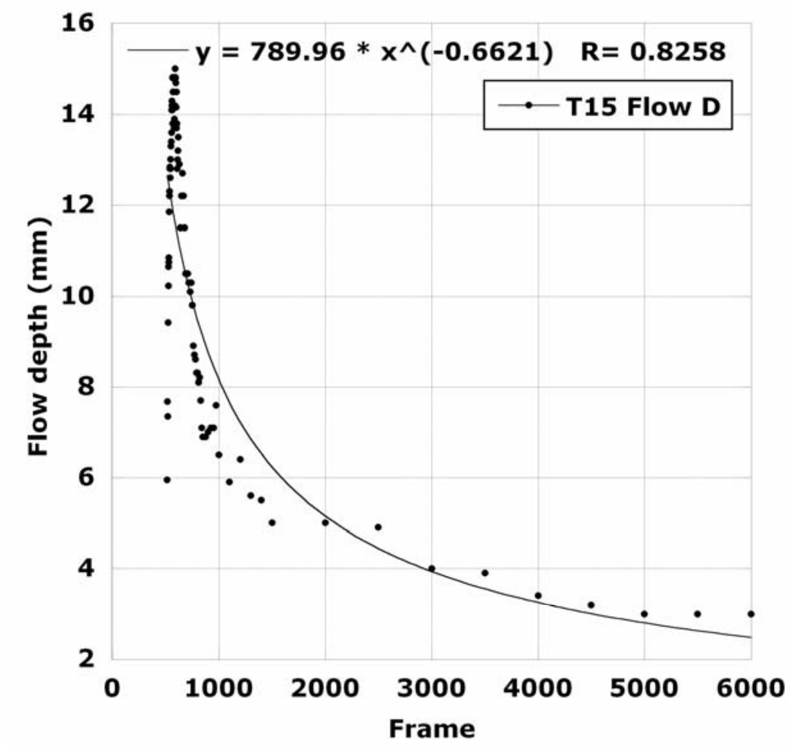

Figure 6 The change in flow depth with time for test T15. This relationship can be approximated with a power law as shown.

2.4.2 Flow velocity

Pore pressure transducers mounted at the base of the flume and high-speed camera data were used to reconstruct the velocity of the flows as they travelled down the flume, as shown in Figure 7. Each pore pressure transducer recorded a spike in pressure as the flow front passed over the sensor. The time between these responses divided by the distance travelled between successive pore pressure transducers gave the average velocity between them. The locations of the data points shown in Figure 7 are half way between the pore pressure transducers which recorded the responses used to calculate the velocity. Figure 7 also shows the front velocity recorded by the high-speed camera near the flume outlet. This velocity was calculated by tracking how long it took the flow front to traverse the width of the camera frame. As shown for test T9, there appeared to be quite good agreement between the velocities measured by the two methods at 420-450 mm. Unfortunately, for the other tests, the final PPT was not functioning, hence we only have the one comparative datapoint.

Both debris flow volume and solid concentration significantly affected flow velocity. For example, the tests conducted with 33% moisture content all show the same general trend; from a near-zero flow velocity at the flume head, where the gradient is 36°, the flow velocity increases to a point nearly half-way down the flume where gradient is 24°, then begins to decelerate as the slope becomes more shallow, down to 12°, at the end of the channel. As expected, an increase in volume causes the velocity to increase. An increase in moisture content has a much more profound effect on velocity, causing the peak velocity to more than double.

The effect of pore fluid type on flow velocity is also striking. For example, comparing test T10 (1.75 kg methyl cellulose) to the equivalent glycerine test (T14) shows a doubling of velocity for the methyl cellulose test (Figure 7). Calculated peak global shear rates are approximately 115 s^{-1} for T14, and 225 s^{-1} for T10. Assuming the influence of global shear rate on fluid viscosity is applies, according to Figure 2, this means the effective viscosity of the pore fluid in the methyl cellulose tests dropped to approximately 33 cP and the resulting effective PSD shifted to the right in terms of consolidation behaviour (i.e. became coarser) by a factor of $(42\text{-}33)^{1/2} = 3$. Such results are applicable to all flows. That is, in each test, regardless of moisture content or volume, the non-Newtonian methyl cellulose flows achieved a velocity of nearly twice their Newtonian counterpart. Reasons for this behaviour are discussed later in this chapter.

Pore pressure data was not available for the erodible bed test (T17, with methyl cellulose pore fluid) as the slightly under-saturated condition of the bed attenuated any pore pressure response at the base. However, the high speed camera images show that the 2.5kg flow with a fixed bed (T7) and erodible bed (T17) have nearly identical velocities at the high speed camera position (note that unfortunately for test T7, the PPTs failed to work, so there is no history of velocity for this test). This was surprising, as we expected that both increased bed roughness and a loss of moisture into the bed would slow the flow, as occurred in previous tests on more unconfined flows (Bowman et al, 2010). Erosion of material from the bed flow may also have caused a change in velocity for test T17, although there is no clear evidence for this here.

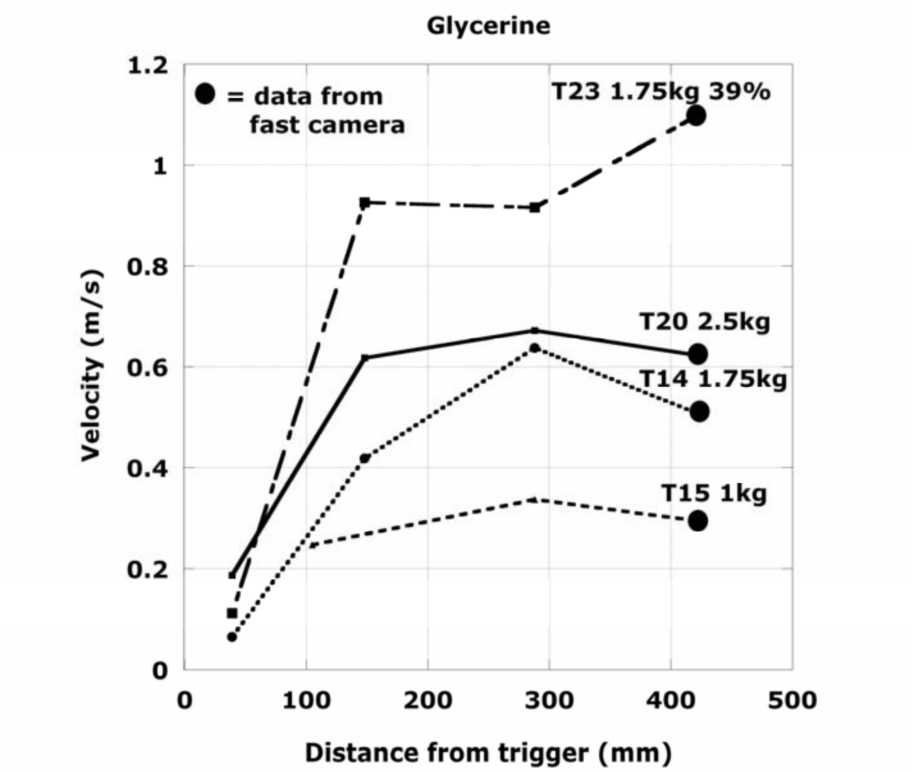

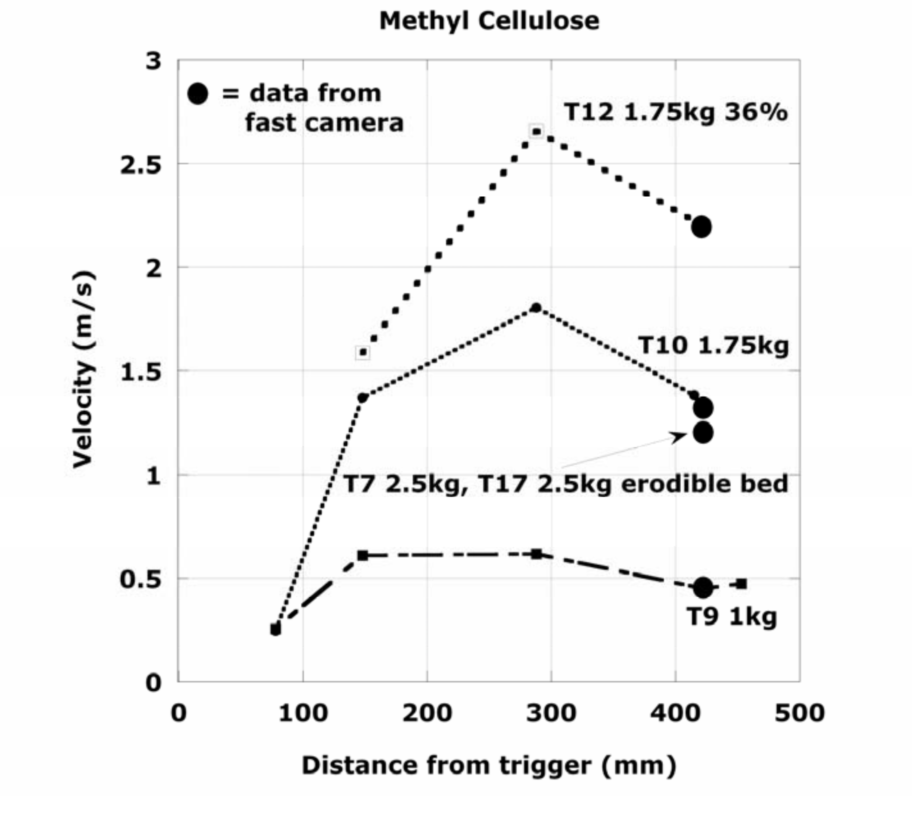

Figure 7: Debris flow velocity versus distance down slope from light barrier. All flows were conducted at 33% moisture content, unless otherwise noted.

2.4.3 Velocity profiles

By tracking particles at various depths as the flow passed by the Perspex window, an attempt was made to reconstruct how velocity changed with depth as the flow front passed. While this was possible for most of the flow depth, unfortunately, the epoxy used to seal the flume and occasional residual material from previous tests obscured the deepest 3 to 4 millimetres of flow, preventing a complete velocity profile to the base of the flume. Figures 8 and 9 show two profiles for each test, one taken at the flow front, while another was taken in the receding limb of the flow hydrograph, but before the transition into the much finer, watery tail portion of the flow.

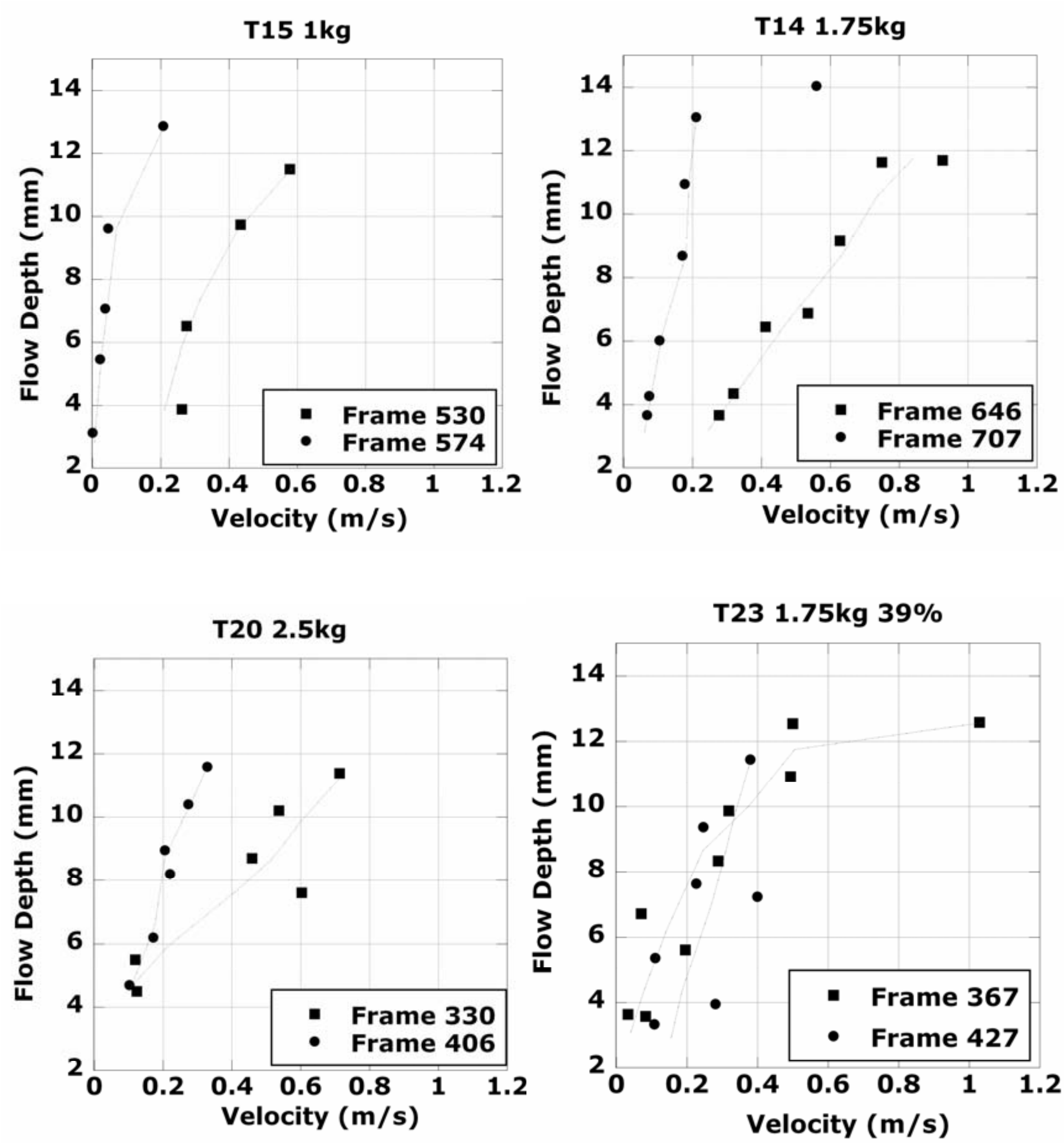

Figure 8 Velocity profiles for glycerine flows. All moisture contents are 33% unless otherwise stated. The first velocity profile (lower frame number) was taken at the true flow front, the second velocity profile(higher frame number) is taken during the falling limb of the hydrograph at a point where enough individual particles could be identified and tracked.

In all tests except T23 and to a lesser extent T12 (both tests with higher moisture content; 39% for T23, using glycerine; 36% for T12, using methyl cellulose) the flow front was found to be much faster and the velocity profile steeper than that observed in the receding limb of the flow. While the flow does slow with time, the dramatic change in profile is caused primarily by friction against the outer walls of the flume. In the true flow front, the flow front represents the velocity profile without the influence of friction from the walls of the flume. In the receding limb, the particles tracked are sliding against the Perspex wall, creating a much steeper velocity profile. The flows with higher moisture content were less frictional, overall between particles, the bottom of the flume, and the sides, thus the differences between flow front and proceeding flow are less dramatic.

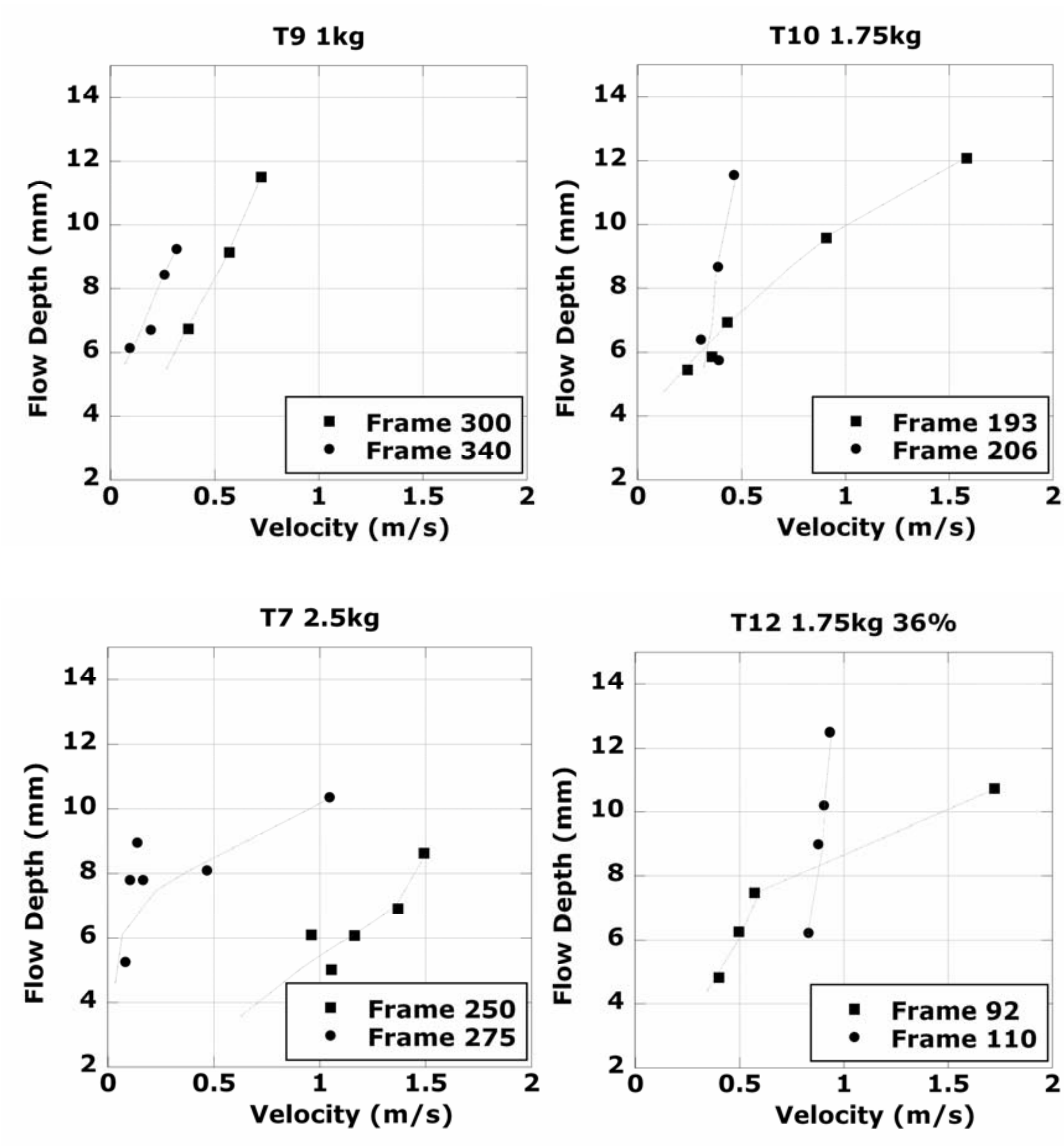

Figure 9 Velocity profiles for methyl cellulose flows. All moisture contents are 33% unless otherwise stated. The first velocity profile (lower frame number) was taken at the true flow front, the second velocity profile(higher frame number) is taken during the falling limb of the hydrograph at a point where enough individual particles could be identified and tracked.

2.4.4 Flow discharge

In order to explore how the discharge of each flow changed with time, hydrographs were constructed for each test, as shown in Figure 10. Each hydrograph was calculated based on an inferred average velocity, flow height, and flow width.

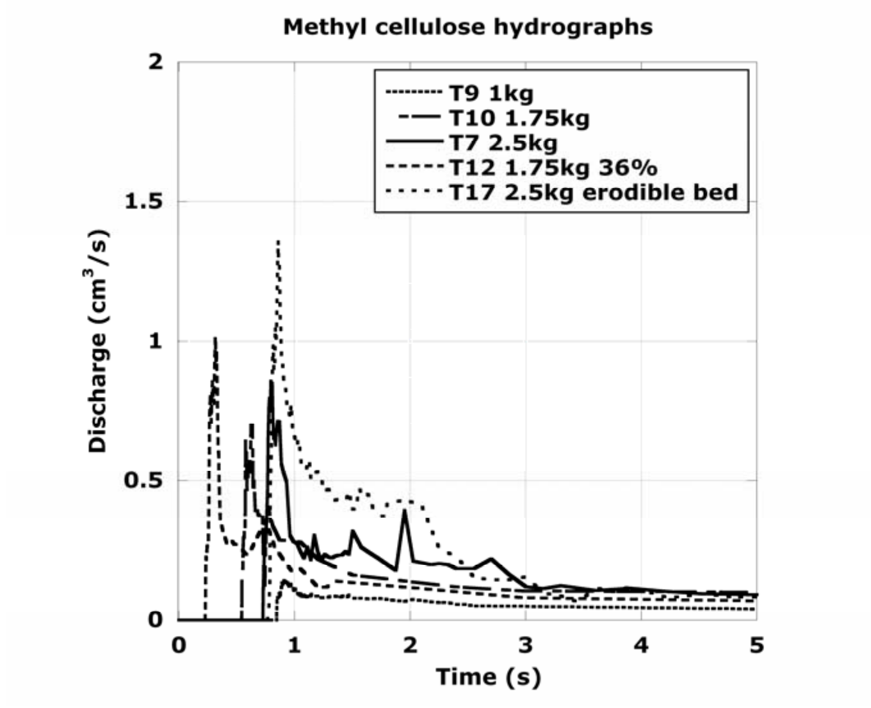

(a)

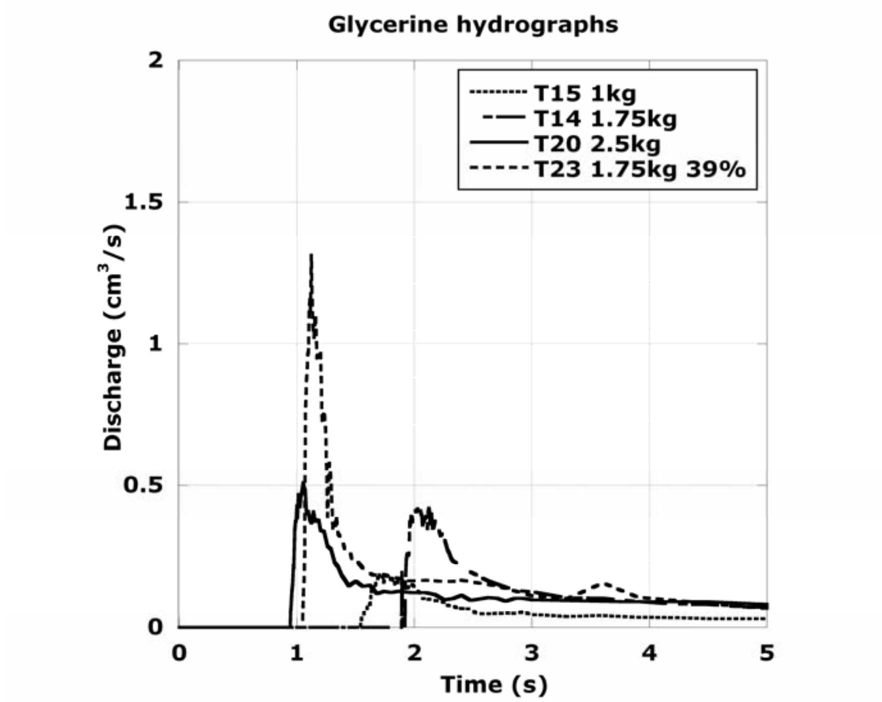

(b)

Figure 10 Discharges for each debris flow test (a) Tests using 33% methyl cellulose as pore fluid. (unless otherwise stated) (b) Tests using 33% glycerine (unless otherwise stated).

Surface flow velocity with depth

The velocity used to calculate the hydrographs was determined by the variation of surface flow velocity with flow depth throughout the duration of a test. In order to explore this relationship, the velocity of between 20 and 30 particles at the surface of the flow was tracked at points in time over the flow duration. Where and when a particle was tracked was determined by the quality of the fast camera imagery, i.e. there had to be enough texture near the surface to actually track one particle for a series of images. Plotting the resulting particle velocities versus their depth showed a moderately linear relationship between flow depth and surface velocity. An example is given in Figure 11 for test T20. Other regression equations developed for each test in the same manner as Figure 10 are given in the final column of Table 3, which is further discussed below.

Flow height

The surface flow height was much easier to determine than surface velocity, as being able to pick out a single particle is not necessary. Flow heights were determined for 60 to 100 frames, depending on the rate of change.

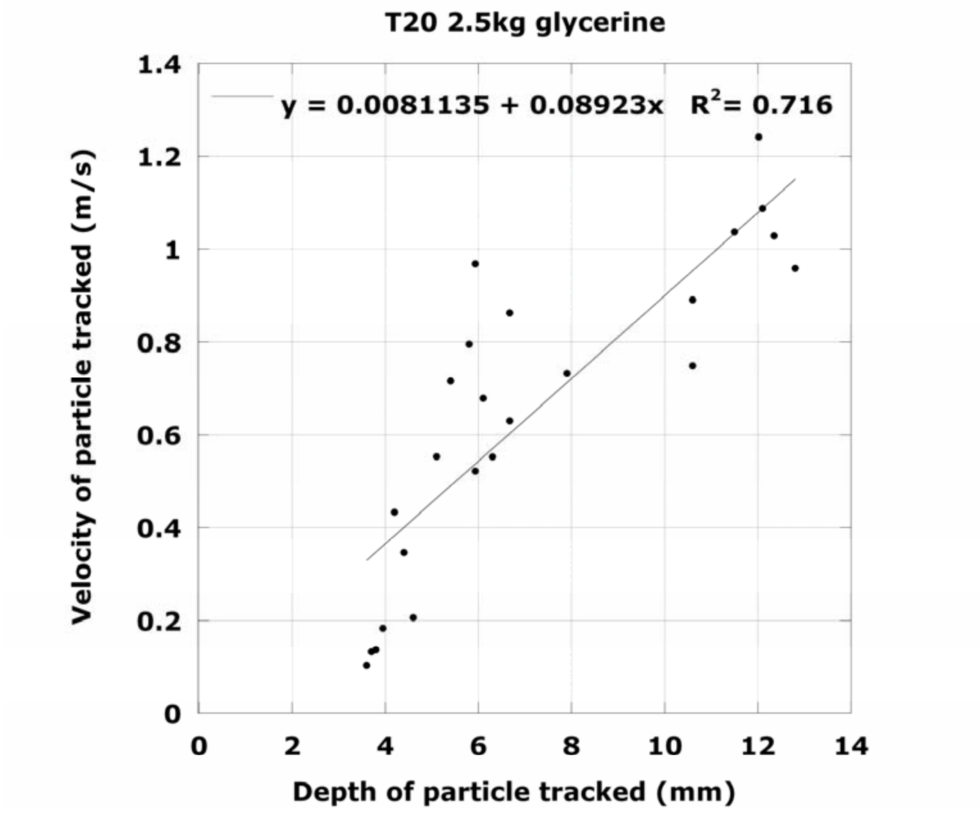

Figure 11 Flow depth versus surface velocity for T20.

Discharge

The flow height data, multiplied by the flow width, gave a cross-sectional area for each frame, but a velocity still had to be determined to calculate a discharge. To do this, the flow height versus velocity relationship discussed above was used (e.g.

Figure 11) to estimate an instantaneous surface velocity for each frame with a flow height data point. Then, a triangular velocity distribution with depth was assumed, as a reasonable first order approximation for a stoney flow based on Takahashi (2007), which is also supported by the profiles given in Figures 8 and 9. Based on this, the average flow velocity is approximately half the calculated surface velocity. By multiplying this average velocity by the cross-sectional area frame by frame, a hydrograph was plotted for each of the tests. The resulting hydrographs were then integrated to calculate a total event volume.

Flow volumes

The total event volumes calculated from the hydrographs, volumes back-calculated from the weight of depositional material collected on the drum surface, and volumes back-calculated from the weight of material entering the flume are shown in Table 3. The calculations assumed a material bulk density of 2.0g/cm^3 for the glycerine flows (weighed wet) and 1.7g/cm^3 for the methyl cellulose flows (weighed dry). The discrepancy between the amount of material entering the feeder tube and the amount of material measured on the depositional surface was sometimes significant, (e.g. up to 33% in test T20). In each test, not all material reached the depositional surface. Some material remained in the feeder tube, some in the flume, and some was lost during the transition from the feeder tube to the head of the flume. In addition, a small amount of material may have been missed in collecting material from the drum surface.

Given the losses in material discussed above, calculated volumes from the hydrograph, in theory, should be less than the volume entering the flume and be greater than the material collected at the drum surface, as some fluid and fine material could not be collected after spin-down due to consolidation. However, the hydrographs do not fully contain the extent of each flow because they are based on high speed camera data only. The high speed camera was only able to record the first 18 seconds of images per test, due to the memory constraints of the in-flight computer, so that in each test, small amounts of flow continued after the last frame. This means that there was an unknown (albeit small) amount of deposition which occurred after the camera had stopped recording that was not taken into account in the hydrograph.

Despite these limitations, the hydrographs lead to some interesting qualitative observations of flow behaviour. As shown in Figure 12, the maximum flow height observed in the glycerine tests varied little, which means that volume and moisture content had very little effect on the maximum cross-sectional flow area observed in the glycerine tests. This suggests that the cross-sectional area of flow was largely limited by the maximum flow rate of the feeder tube. Given that the maximal cross-sectional area of each of the tests was similar, velocity at the camera position was the major factor in determining peak discharge.

As also shown in Figure 12, the flow heights of the methyl cellulose tests were slightly lower than the glycerine tests and the hydrographs in Figure 10 show a sharper peak discharge with a steeper receding limb for the methyl cellulose tests. Faster flows appear to show more abrupt peak discharges, as the entire flow front moves much faster.

Table 3 Compares different measurements for each flow and the relationship between surface velocity and flow height. Volume of deposition (column 2) was calculated from point measurements of depth. Column three was calculated from the hydrograph. The volume entering the flume was back calculated from the weight of material prepared versus the weight of material that was retained in the mixing container after the test, using a density of 2.0g/cm^3).

Test	Volume of deposition (cm^3)	Volume of deposition from hydrograph (cm^3)	Hydrograph / measured deposition (%)	Calculated / volume entering flume (inferred)	Surface velocity (mm/s) = f (flow height)
T7	1,119	1,300	116%	73%	$y = 69.661x + 88.674$ $R^2 = 0.3821$
T9	425	466	110%	72%	$y = 116.29x + 561.12$ $R^2 = 0.4492$
T10	747	1,100	147%	87%	$y = 125.82x + 305.89$ $R^2 = 0.491$
T12	697	1,182	170%	93%	$y = 197.47x + 69.082$ $R^2 = 0.3485$
T14	855	816	95%	74%	$y = 90.107x - 106.05$ $R^2 = 0.7859$
T15	497	449	90%	72%	$y = 26.265x + 87.257$ $R^2 = 0.668$
T17	1,227	1,762	144%	98%	$y = 122.68x + 917.72$ $R^2 = 0.3038$
T20	1,144	1,112	97%	67%	$y = 89.23x + 8.1135$ $R^2 = 0.716$
T23	889	1,209	136%	99%	$y = 129.52x - 157.04$ $R^2 = 0.6875$

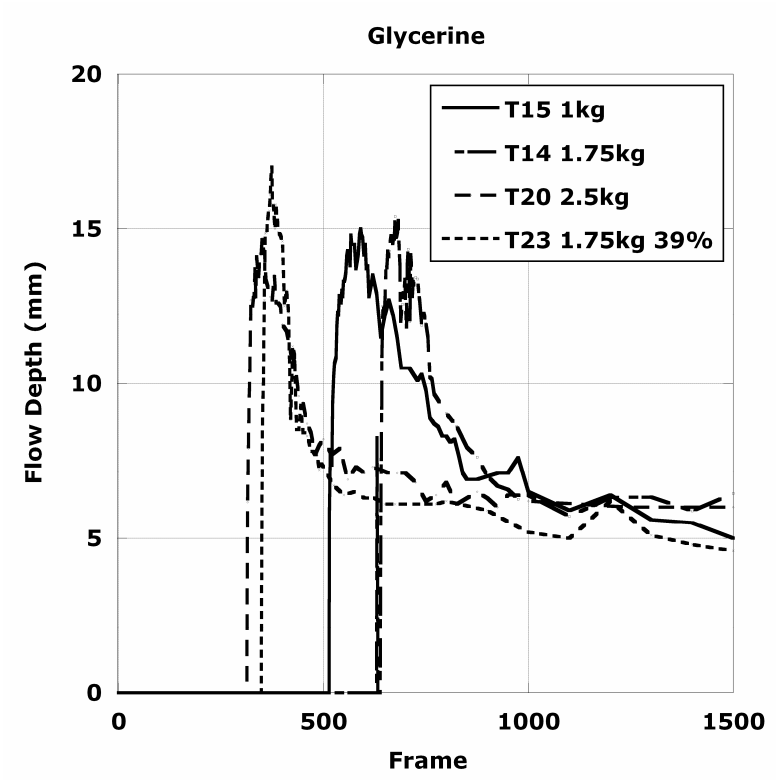

(a)

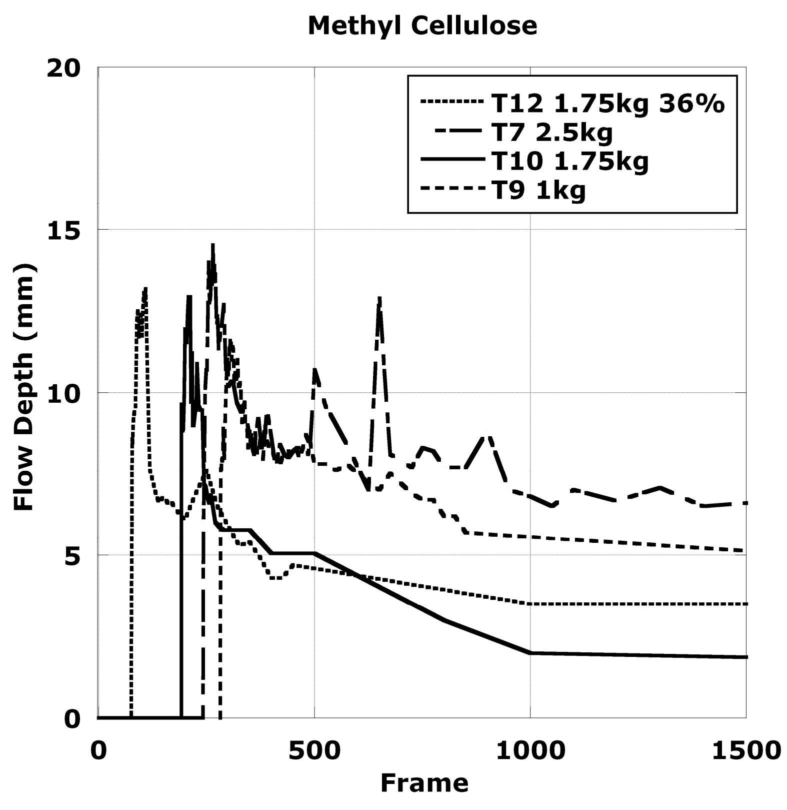

(b)

Figure 12 Flow depths versus frame. (a) Glycerine (b) Methyl Cellulose The passage of the coarse flow front corresponds to the spike. The transition to the finer tail corresponds to point where the change in flow height suddenly decreases.

As well as the quantitative differences in flow height behaviour between tests, there was an observed qualitative difference in flow width between tests conducted using the glycerine and using methyl cellulose, whereupon lateral levees were found to form during the methyl cellulose tests.. For example, both tests T7 and T9 were effectively unchannelized. Based on the high speed camera images, material at the lateral part of the flow near the Perspex window was observed to slow, then stop entirely. This lateral levee effectively decreased the channel width. Therefore, in constructing the hydrographs, a narrower, approximate channel width was used, less than the full 60mm for the glycerine tests (40mm in the case of test T9, 60mm progressing down to 30mm over time, in the case of test T7). It is also possible that this was the case in the other tests as well, but material slowed and stopped on the other side of flume and the effect was not visible in the Perspex window. This may help to explain why the calculated event volumes from tests T10 and T12 hydrographs overestimate the deposition. Further, since the methyl cellulose tests ran out less on the drum surface, material from the watery tail was observed to back up into the flume. This material was not taken into account in the depth measurement of the material deposited on the fan. This may also help to explain the difference between the calculated material passing the camera frame from the hydrograph and the amount of material deposited (see Table 3).

2.4.5 Runout and deposition

Contour plots

Point measurements of depth through the consolidated deposit zone after spin down of the centrifuge were used to construct contour plots of the deposition fan – Figures 13 to15. The morphology of deposition was similar in all tests. In contrast to many debris flows mapped in the field, the width of lateral spread exceeded the runout of deposition. This is likely to be due to the rapid deceleration of the flow within the channel, leading to deposition within it before opening to a horizontal unconfined fan zone (in terms of prototype). This is explained by the slope profile of the channel. While the channel slope angle averaged 24°, it continuously reduced from the head at 36° to the base at 12°, which is typical for a fan slope angle in the field. However, in this case,,the flow was still confined within the channel. Fannin and Wise (2001) suggest, based on a dataset of debris flows from British Columbia, that within confined channels, deposition may occur at slope angles below 9°, whereas for transition zones (at the transition between the end of a confined channel and head of a fan), deposition may occur on slopes below 20° to the horizontal. The end of slope angle lies between these two values and deposition on the fan was noted to back up as far as the camera position at latter stages of the flows.

As expected from the velocity data and data obtained previously (Bowman et al, 2010), depositional area increased with both increased volume and moisture content. However, the effect of increased moisture content was found to be much more important than an increase in volume. For example, the overall deposition area between tests T20 (2.5 kg at 33% moisture content) and T23 (1.75 kg at 39% moisture content) was nearly identical, despite the fact that T20 was 50% larger in mass than T23 (Figure 11). Furthermore, the higher mobility provided by the higher water content of test T23 allowed it to spread thinner and farther than a flow of the same volume and lower moisture content (test T14 at 33%).

Comparing equivalent plots for mass and moisture content between Figure 13 (glycerine tests) and Figure 14 (methyl cellulose tests), shows that the deposition morphology for the glycerine based tests was virtually the same as for the methyl cellulose tests, However, the erodible bed test using in methyl cellulose (Figure 15) notably showed an increased inundated area over the non-erodible bed tests.

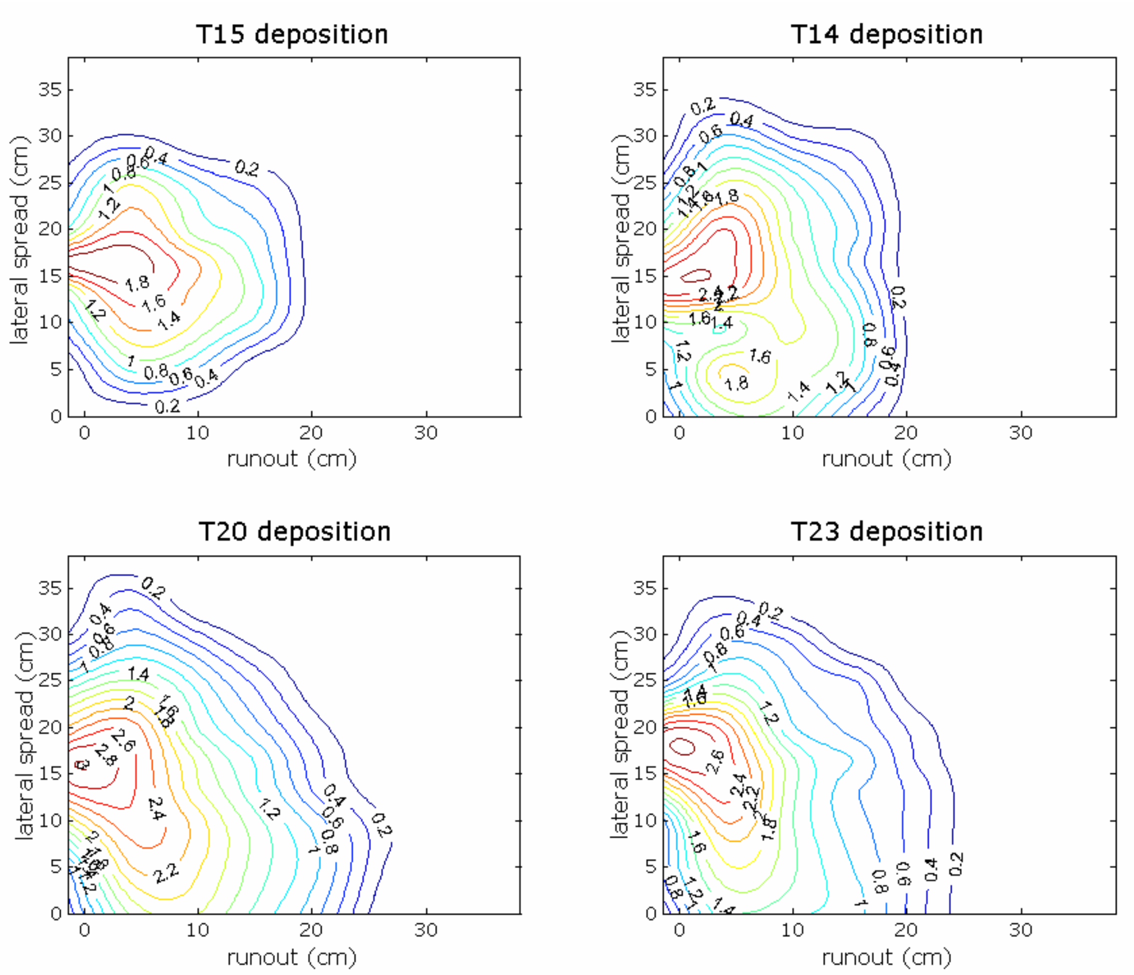

Figure 13 Deposition morphology for glycerine tests

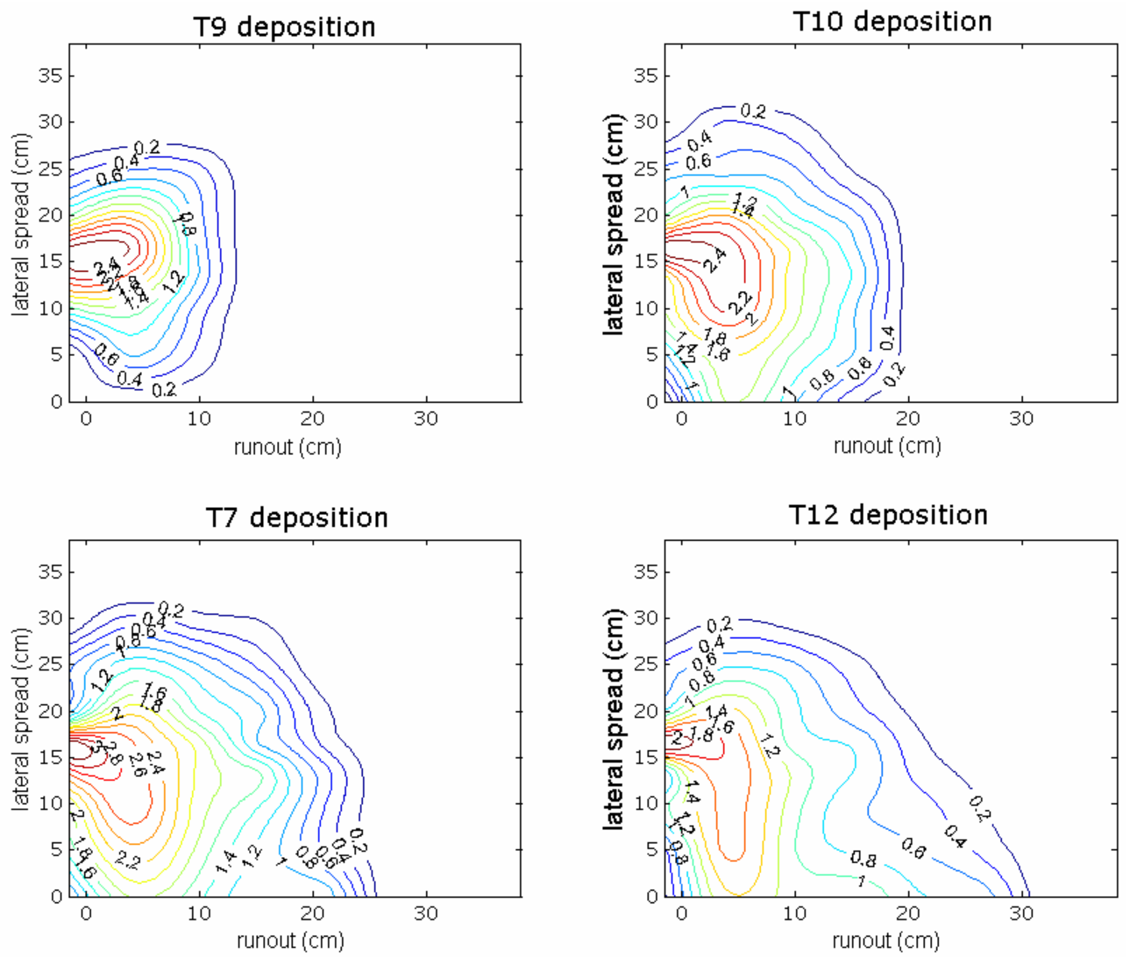

Figure 14 Deposition morphology for methyl cellulose tests

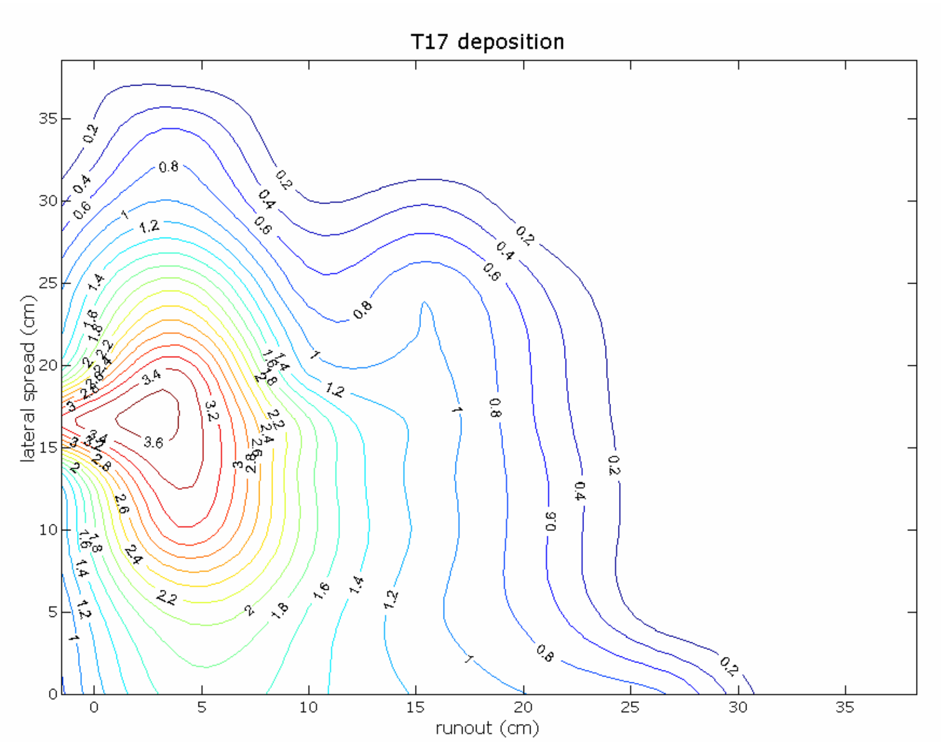

Figure 15 Deposition morphology for erodible bed test, T17 with 2.5kg and 33% moisture content.

Centre of gravity of deposition fan

The edges of the contour plots (i.e. plan area of deposition), while useful for visualizing the morphology of the deposit, were not well suited to analyzing debris flow runout. For this reason, the centre of gravity was calculated for each flow from the contour plots.

As shown in Figure 16, for each flow fluid rheology, approximately linear relationships were observed to exist between flow mass and runout to the centre of gravity for flows conducted at a moisture content of 33%. The relationship between flows using methyl cellulose and glycerine was different, with a stronger correlation for glycerine, however, the same overall trends were observed, with a high correlation coefficient for both. In both cases, the relationship changed with the moisture content of the flow, so that flows of a higher moisture content produced a higher runout than predicted by the trendline for 33%. The erodible bed test plotted close to the 33% moisture content line for the methyl cellulose pore fluid, suggesting that it behaved very similarly to the test conducted without an erodible bed (this is supported by the data in Figure 7, showing similar velocities for both tests at the camera).

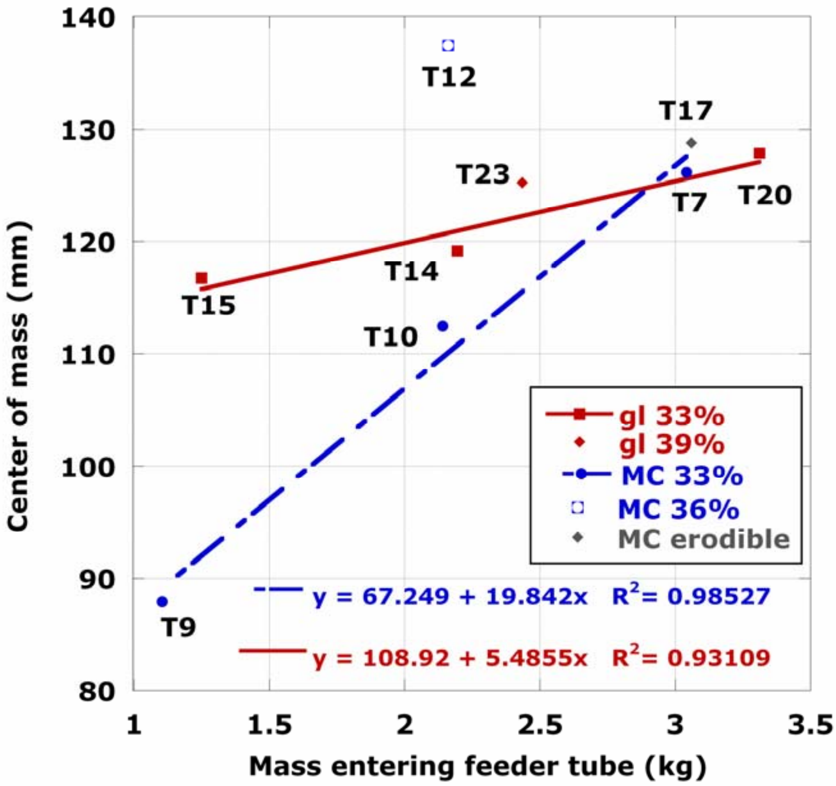

Figure 16 Plot of the centre of mass versus mass entering the feeder tube.

As shown in Figure 17, an approximately linear relationship was also observed to exist between the square of velocity and centre of gravity (after Hungr et al. 1984; Takahashi, 1997) for flows at a moisture content of 33%, for each flow rheology. However, again, test flows conducted at a higher moisture content did not plot on the same relationship. Instead a higher moisture content, which led to a higher velocity at the observation point in the channel, did not lead to as much runout as predicted by the plotted trend. Correlation coefficients, at R^2 of 0.85 and 0.76 for glycerine and methyl cellulose, respectively, were not as high as for the relationship between mass (or volume) and runout.

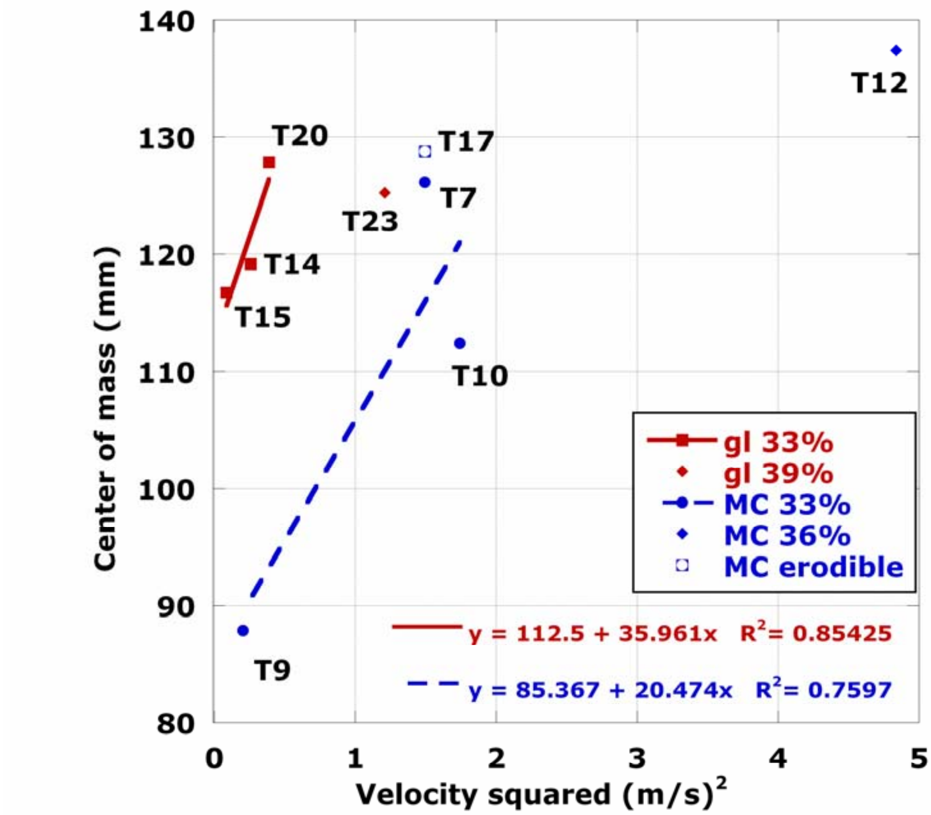

Figure 17 Location of the centre of mass of the deposition (from flume outlet) versus the square of velocity at the fast camera position.

Figure 18 shows peak momentum of the flow, calculated as the total mass entering the flume (kg) multiplied by the flow front velocity at the camera (m/s) against position of the centre of gravity. Two trends are plotted for each fluid rheology – one includes only the data taken at 33% moisture content, the other includes all data (tests at higher moisture content and, for methyl cellulose, the erodible bed test). This figure shows the best linear correlation obtained for the 33% moisture content tests (R^2 of 0.94 and 0.99, for glycerine and methyl cellulose, respectively). It also shows that data can be collapsed to a single trendline for each rheology, in which moisture content and erodible / non-erodible beds are included (with R^2 of 0.80 and 0.99 for glycerine and methyl cellulose, respectively). It is particularly interesting that the methyl cellulose tests, in which the runout which did not correlate so well with either the square of velocity or total mass, collapses so well to a relationship with peak momentum. This may be because the peak moment includes both velocity and total mass in its derivation.

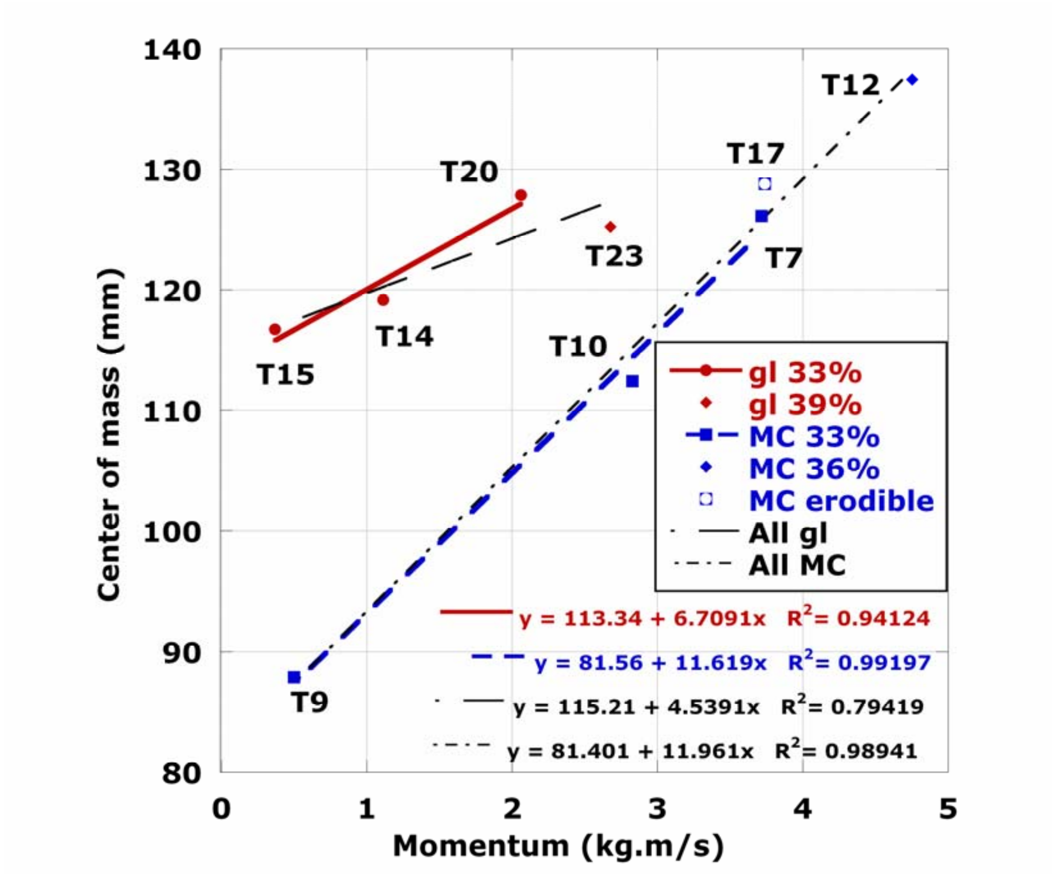

Figure 18 The runout of each test (shown by the distance of its centre of mass from the flume outlet) versus the peak momentum of the flow at the fast camera position.

Perhaps the most interesting observation overall from Figures 16 to 18 is the effect of using different pore fluids. While the runout of each test appears to be largely controlled by peak flow momentum, the relationship is different between the two rheologies. For a given momentum, the methyl cellulose flows runout far less than their glycerine counterpart. Further, an increase in momentum increases the runout more for a methyl cellulose flow than for a glycerine flow (evinced by a steeper linear curve fit).

2.5 Discussion and conclusions

The nine geotechnical centrifuge tests summarized in this chapter demonstrate several important aspects of debris flow behaviour. They also highlight some of the advantages and challenges of modelling debris flows in a geotechnical centrifuge.

- Nine debris flow tests conducted in a geotechnical centrifuge are discussed here, which employed variable volumes and moisture contents, at a rotational velocity to produce an acceleration field equivalent to 40g. Two different pore-fluids were used to test the effect of pore fluid rheology on flow behaviour. Pore pressure and high-speed camera data were used to construct plots of flow velocity with distance, flow height over time, velocity profiles with depth, and discharge over time.

- Both an increase in volume and an increase in moisture content resulted in an increase in peak velocity during down-slope movement. However, the effect of increasing the moisture content of the flow was found to be much more pronounced than that of increasing the flow volume. The maximum cross-sectional area observed was most likely limited by the flow diameter of the feeder tube. Consequently, flow velocity largely determined the peak discharge of each flow. The use of a non-Newtonian pore fluid increased velocity downslope by a factor of two.

- The large difference between the measured velocity profiles at the flow front and during the recessional phase of the flow (but still in the coarse front) is explained by a general trend of decreasing velocity with time and friction against the flume walls. An increase in moisture content increased the mobility of the flow in terms of inundated depositional area and runout.

- Correlations were found between square of velocity of the flow front at the camera position and runout and also between total mass and runout, although these relationships only held for particular sets of conditions. However, the runout of all flows of a given pore fluid rheology appeared to be linearly related to the peak momentum of the flow at the flume outlet as defined by the product of flow front velocity and total flow mass. This is a particularly interesting result, although should be treated with caution on two fronts. The first is that the boundary conditions include a peak flow rate that is limited by the geometry of the feeder tube to the head of the flume, so that the relationship should be checked against other flow conditions that do not have this restriction. The second is that, while flow momentum may turn out to be a better parameter to correlate to runout than is either velocity or mass, practically speaking, the information available in the field often is either total mass (i.e. taken from the deposit volume after the event) or velocity (i.e. from eyewitness accounts or run-up measurements), and rarely is both.

- Different runout versus momentum relationships were observed for the two fluid types. The non-Newtonian flows ran out less for a given momentum than an equivalent flow with Newtonian pore fluid. That is, during downslope motion, the methyl cellulose flows were more mobile (faster) as a consequence of a lower pore fluid viscosity at high shear rates despite the drop in viscosity also leading to an increased rate of consolidation This suggests that the glycerine flows were made relatively slower by greater viscous shearing or drag during the acceleration phase.

As the flows decelerated, a different response was observed. Between the position of velocity measurement and flume outlet, the methyl cellulose decelerated faster than the glycerine flows, creating levees within the channel at the sides of the flows in at least two tests. Deceleration would have led to an increase in viscosity and a subsequent decrease in consolidation rate – the former leading to a greater deceleration, and the latter leading to a reduced deceleration. Given that deceleration was, overall, greater for methyl cellulose than for glycerine flows this suggests that viscous effects, which are greater than for glycerine at low shear rate, dominated over consolidation effects in this case.

These results finds agreement with previous work on the modelling of models for debris flows, in which Bowman et al (2010) found good agreement in terms of velocity between downslope motion of flows matched for consolidation (i.e. by scaling viscosity with N), however, the runout was slightly less for those tests using a more viscous fluid (at correspondingly higher N). Borrowing from the soil dynamics literature, Bowman et al (2010) suggested that the downslope (accelerating) motion and runout (decelerating) motion of a debris flow may be considered as experiencing a "forced vibration" phase (as the flow runs down the flume with energy being input to the system) and a "free vibration" phase (as the flow runs out onto the drum surface while no more energy is supplied). The flow behaviour in this series of tests lends support to the notion that viscous forces may act to inhibit consolidation to a point and promote lateral spreading, but beyond this, may also apply drag to soil particles, inhibiting their motion and reducing runout. Alternatively, for coarse grained flows with low viscosity interstitial fluids, consolidation is likely to be the dominant mechanism of flow arrest. For debris flows that exhibit both frictional and viscous characteristics, therefore, it may not be clear which mechanism controls acceleration and deceleration. Indeed, if the dominance of different mechanisms of shear resistance shifts between channelized down-slope movement and unconfined runout, this will have important implications for both the understanding and modelling of debris flow mechanics.

Acknowledgements

This research made possible by a New Zealand Earthquake Commission Bie-anniual grant, athe University of Canterbury Doctoral Scholarship, and a New Zealand Postgraduate Study Abroad Award. Thanks go to members of the geotechnical group at ETH, Zurich, for their patience and generosity – in particular, Jan Laue, Sarah Springman, Heinz Buschor, Bernd Imre, Ralf Herzog, Marco Sperl, and Anita Meyer. A debt of gratitude is owed especially to Markus Iten, who was indispensable and irreplaceable both before, during and after the experiments.

REFERENCES

Benda, L., and Dunne, T. 1997. Stochastic forcing of sediment supply to channel networks from landsliding and debris flow. Water Resources Research, **33**(12): 2849-2863.

Benda, L., and Sias, J. 2003. A quantitative framework for evaluating the mass balance of in-stream organic debris. Forest Ecology and Management, **172**(1): 1-16.

Bowman, E.T., and Sanvitale, N. 2009. The role of particle size in the flow behaviour of saturated granular materials. *In* 17th International Conference on Soil Mechanics and Geotechnical Engineering. *Edited by* M. Hamza, S. Marawan, and Y. El-Mossallamy. Alexandria. Millpress, Vol.1, pp. 470-473.

Bowman, E.T., Imre, B., Laue, J., and Springman, S.M. 2007. Geotechnical centrifuge modelling of debris flows. *In* The Fourth International Conference on Debris-flow Hazards Mitigation: Mechanics, Prediction, and Assessment. Millpress, Chengdu, China, p. 229 to 239.

Bowman, E.T., Laue, J., Springman, S., and Emre, B. 2010. Experimental modelling of debris flow behaviour using a geotechnical centrifuge. Canadian Geotechnical Journal.

Bowman, E.T., Laue, J., Imre, B., Zweidler, A., and Springman, S.M. 2006. Debris flows in a geotechnical centrifuge. *In* International Conference on Pysical Modelling in Geotechnics, Hong Kong, China, pp. 311-316.

Chikatamarla, R., Laue, J., and Springman, S.M. 2006. Centrifuge Scaling laws for guided free fall events including rockfalls. International Journal of Physical Modelling in Geotechnics, **6**(2): 15-26.

Craig, W.H., James, R.G., and Schofield, A.N. 1988. Centrifuges in Soil Mechanics. A.A. Balkema, Rotterdam.

D'Agostino, V., Cesca, M., and Marchi, L. 2010. Field and laboratory investigations of runout distances of debris flows in the Dolomites (Eastern Italian Alps). Geomorphology, **115**(3-4): 294-304.

Garnier, J., Gaudin, C., Springman, S.M., Culligan, P.J., Goodings, D., Konig, D., Kutter, B., Phillips, R., M.F., R., and Thorel, L. 2007. Catalogue of scaling laws and similitude questions in centrifuge modelling. International Journal on Physical Modelling in Geotechnics, **7**(3): 1-24.

Hungr, O., Morgan, G.C., and Kellerhals, R. 1984b. Quantitative analysis of debris torrent hazards for design of remedial measures. Canadian Geotechnical Journal, **21**: 663-677.

Hungr, O., Evans, S.G., Bovis, M., and Hutchinson, J.N. 2001. Review of the classification of landslides of the flow type. Environmental and Engineering Geoscience, **7**: 221-238.

Iverson, R. 2003. The debris-flow rheology myth, pp. 303–314.

Iverson, R., and Denlinger, R. 2001. Flow of variably fluidized granular masses across three-dimensional terrain: 1. Coulomb mixture theory. J. Geophys. Res, **106**: 537-552.

Iverson, R., M. 2005. Debris-flow mechanics. *In* Debris-flow Hazards and Related Phenomena. Praxis, Chichester. pp. 105-134.

Jakob, M. 2005. A size classification for debris flows. Engineering Geology, **79**(3-4): 151-161.

Kutter, B. 1995. Recent advances in centrifuge modeling of seismic shaking. *In* 3rd International Conference on Recent Adavances in Geotechnical Earthquake Engineering and Soil Dynamics. St. Louis, Missouri. April 2-7, 1995, pp. 927–941.

Phillips, C.J., and Davies, T.R.H. 1991. Determining rheological parameters of debris flow material. Geomorphology, **4**(2): 101-110.

Pierson, T. 1980. Erosion and deposition by debris flows at Mt. Thomas, North Canterbury, New Zealand. Earth Surface Processes, **5**: 227-247.

Rickenmann, D. 1999. Empirical Relationships for Debris Flows. Natural Hazards, **19**(1): 47-77.

Rickenmann, D. 2005. Runout prediction methods. Debris-Flow Hazards and Related Phenomena: 263-282.

Schofield, A.N. 1980. Cambridge Geotechnical Centrifuge Operations. Géotechnique, **30**(3): 227-268.

Springman, S., Laue, J., Boyle, R., White, J., and Zweidler, A. 2001a. The ETH Zurich geotechnical drum centrifuge. International Journal of Physical Modelling in Geotechnics, **1**(1): 59-70.

Takahashi, T. 2007. Debris flow: mechanics, prediction and countermeasures. Routledge.